Arterial Spin Labeling Perfusion of the Brain: Emerging Clinical Applications

Sven Haller MD, MSc

Greg Zaharchuk MD, PhD

David L Thomas PhD

Karl-Olof Lovblad MD

Frederik Barkhof MD

Xavier Golay PhD

Affidea Centre Diagnostique Radiologique de Carouge, Clos de la Fonderie 1, 1227 Carouge, Switzerland (S.H.); Dept of Surgical Sciences, Div of Radiology, Uppsala Univ, Sweden (S.H.); Dept of Neuroradiology, Univ Hosp Freiburg, Germany (S.H.); Faculty of Medicine Univ of Geneva, Switzerland (S.H.)

Dept of Radiology, Stanford University, Stanford, CA, USA (G.Z.)

University College London, Institute of Neurology, London, UK (D.L.T., X.G.)

Dept of Diagnostic and Interventional Neuroradiology, Geneva University Hospitals, Switzerland (K.O.L.)

Dept of Radiology & Nuclear Medicine and PET Research, VU University Medical Centre, Amsterdam, The Netherlands (F.B.); and Institutes of Neurology and Healthcare Engineering, University College London, England (F.B.)

Address correspondence to:
Sven Haller sven.haller@gmail.com

Supported in part by COST Action BM1103 on ASL in dementia

ABBREVIATED TITLE PAGE

Manuscript title

Arterial spin label perfusion of the brain: emerging clinical applications

Manuscript type

Review

Essentials

- Due to the close link between brain metabolism and perfusion, patterns of FDG PET closely resemble those of ASL (page 11)
- ASL complements structural information of standard MRI in neurocognitive decline and may allow early diagnosis of dementia (page 11)
- ASL may detect mismatch perfusion in acute stroke, and identify tissue at risk in chronic cerebrovascular disease (page 13)
- ASL may detect arterio-venous shunting in arterio-venous malformation and fistulas (page 16)
- ASL may be used to localize the epileptogenic focus in seizure disorders (page 17).
- In neoplasms, ASL may replace standard Gadolinium enhanced dynamic susceptibility contrast (DSC) notably in patients with allergies, renal insufficiency or children (page 18)
- ASL may detect subtle functional changes in psychiatric disorders such as post-traumatic stress disorder or mild traumatic brain injury, where standard structural MRI typically provides no detectable anomaly (page 21)
- Emerging new applications of ASL include super-selective ASL to map vascular territories and cerebrovascular reserve imaging (page 32)

Disclosure

No conflicts of interest

Abstract

Arterial spin labeling (ASL) is an MR imaging technique used to assess cerebral blood flow (CBF) non-invasively by magnetically labeling inflowing blood. In this article we review the main labeling techniques, notably pulsed and pseudo-continuous ASL as well as emerging clinical applications. In dementia, the pattern of hypoperfusion on ASL closely matches the established patterns of hypometabolism on FDG-PET due to the close coupling of perfusion and metabolism in the brain. This suggests that ASL might be considered as an alternative for FDG, reserving PET to be used for the molecular disease-specific amyloid and tau tracers. In stroke, ASL can be used to assess perfusion alterations both in the acute and the chronic phase. In arteriovenous malformations and dural arteriovenous fistulas, ASL is very sensitive to detect even small degrees of shunting. In epilepsy, ASL can be used to assess the epileptogenic focus, both in the peri- and inter-ictal period. In neoplasms, ASL is of particular interest in cases in which gadolinium-based perfusion is contraindicated (e.g., allergy, renal impairment) and holds promise to differentiate tumor progression from benign causes of enhancement. Finally, various neurologic and psychiatric diseases including mild traumatic brain injury or posttraumatic stress disorder display alterations on ASL images in the absence of visualized structural changes. In the final part, we review current limitations and future developments of ASL techniques to improve clinical applicability, such as multiple inversion time ASL sequences to assess alterations of transit time, reproducibility and quantification of CBF, and to measure cerebrovascular reserve.

Abbreviations

AD	Alzheimer disease
ASL	arterial spin labeling
BOLD	blood oxygen level-dependent (effect)
CT	computed tomography
CTP	computed tomography perfusion
DSC	dynamic susceptibility contrast (perfusion)
EPI	echo planar imaging
FDG	18F-2-fluoro-2-deoxy-D-glucose
GRASE	gradient and spin echo
MCI	mild cognitive impairment
MRI	magnetic resonance imaging
MT	magnetization transfer
PET	positron emission tomography
PLD	post-labelling delay
relCBF	relative cerebral blood flow
RF	radio-frequency
SNR	signal to noise ratio
TI	inflow time

Introduction

Arterial spin labeling (ASL) is an MR imaging technique that enables the measurement of brain perfusion non-invasively at the tissue level. Benefiting from the contrast of inflowing magnetically-labeled blood, ASL obviates the need for an exogenous contrast agent. Although the principle of ASL was introduced in early 1990s (1-3) and is feasible on low-field MR systems, ASL greatly benefits from the improved signal-to-noise ratio (SNR) of modern high-field MRI systems (4). The increasing availability of 3T scanners as well as the development of improved pulse sequences and multi-channel receiver array coils has led to a rapidly growing interest in ASL within the past few years, paving the way for widespread application in neurological and psychiatric disorders. The current review will start by briefly summarizing the essential technical requirements, and then discuss in more detail emerging clinical applications of ASL (such as dementia, stroke, vascular malformations, epilepsy, tumors and psychiatry), and concludes with a critical review of the current limitations and future perspectives of brain ASL imaging.

Essential technical considerations

Basic Concepts of ASL

ASL is based on the principle of magnetically labeling inflowing arterial blood protons prior to their entry into the tissue of interest. As such, it can be viewed as a tracer technique (5, 6), with water acting as the natural endogenous tracer to estimate tissue perfusion. The label is created by applying radio-frequency (RF) pulses to invert the bulk magnetization of the blood water

protons. Images are acquired after the labeling and inflow period using rapid acquisition techniques such as echo-planar imaging (EPI), gradient and spin echo (GRASE) imaging, or 3-dimensional fast spin-echo (3D-FSE) imaging using a stack-of-spirals approach (7-9). A pair of images is always acquired: a labeled image, in which the blood water magnetization is inverted, and a control image, in which the blood water magnetization is not inverted. The signal difference between labeled and control images is proportional to the amount of magnetization inverted and delivered to the tissue. If all the labeled blood has arrived at the imaging voxel at the time of image acquisition, the signal difference will be proportional to cerebral blood flow (CBF). The current main implementations of ASL are pulsed and pseudo-continuous labeling.

Pulsed ASL

In PASL, the arterial blood water is labeled using a short adiabatic inversion pulse. The labeling pulses are on the order of ~10ms and designed to invert the blood water instantaneously in a particular region, typically located inferior to the brain (Figure 1A). After labeling, a post-label delay period is required (also known as the inflow time or TI for PASL), during which time the inverted blood moves from the labeling region into the brain, loosing gradually its label through longitudinal T1 relaxation. For this reason, PASL is intrinsically a lower SNR technique than is pseudo-continuous ASL (pCASL). The control acquisition for PASL consists of applying an RF pulse with equivalent power to the labeling pulse, but which has a net zero effect on the blood water magnetization in the labeling region.

Pseudo-continuous ASL

In pCASL, a long labeling period (1-2 sec) is made up of a train of very short (≈1ms) pulses (9). This train of short pulses is designed to invert the inflowing blood magnetization in an adiabatic or pseudo steady-state manner (Figure 1B). It is useful to think of the blood being continuously inverted as it flows through a 'labeling plane' in the inferior-superior direction. If the phase of every second pulse in the pCASL pulse train is shifted by 180°, the flowing blood water is minimally perturbed, and thus enables acquisition of non-labeled control images. pCASL has recently been adopted as the labeling method of choice for clinical imaging, due to its ease of implementation and high SNR (10).

Pros and cons: PASL vs pCASL

The main advantage of pCASL over PASL is its higher SNR - a substantial benefit in a technique that is intrinsically SNR-limited. The reason for this can be understood by considering the degree of labeling of the arterial blood as it arrives at the tissue, and how this changes during the inflow time and/or post-labeling delay (Figure 2). For PASL, a slab of arterial blood is inverted at TI=0, and subsequently undergoes T1 relaxation during the inflow time. For pCASL, the arterial blood is continuously inverted as it passes through the labeling plane, which means that all the blood has the same amount of T1 decay when it arrives at the tissue, irrespective of when it was labelled. However, the benefits of pCASL are not as large in practice as would be predicted theoretically, due to: (i) the inversion efficiency of the RF pulses used in PASL, higher than that achieved using the pCASL flow-induced adiabatic

inversion pulse train; (ii) the sensitivity of the pCASL labeling train to off-resonance effects, which can cause apparent regional hypoperfusion if different feeding arteries are affected differently; (iii) the longer arterial arrival times for pCASL for which the labeling plane is required to intersect major feeding arteries with flow in a known direction, generally placed distally to the PASL labeling slab. Consequently, for any given study, it is always worth considering the specific pros and cons of pCASL and PASL in order to choose the most appropriate option.

The critical importance of the Post-label delay time

An important aspect of all ASL techniques is the introduction of the PLD (or TI) between the end of the labeling pulse and the time of image acquisition (11). If the PLD is longer than the longest transit time between the tagging plane and the imaging volume, the ASL signal becomes insensitive to variations in arterial arrival time, as long as the blood and tissue T1 values are similar (true for grey matter but not white matter) (11, 12). This enables cerebral blood flow (CBF) quantification and minimizes the appearance of intravascular signal in the ASL images, yet at the expense of SNR, due to the T1 relaxation of the bolus ($T1_{blood}$=1600ms at 3T). In addition, the choice of PLD depends on the subject's age, with older subjects showing longer arterial arrival times. The recommended PLD for pediatric and adult clinical populations are 1500 ms and 2000 ms, respectively (10).

Alterations of transit time - multi TI ASL

Most clinically available ASL sequences use only a single delay between labeling and image acquisition, based on original values calculated from healthy young adults. In case of proximal vessel occlusion, there is a delayed arrival of blood in the parenchyma, which may falsely suggest a reduced relative CBF as estimated by ASL (Figure 3) (13) and increased ASL signal in the feeding arterial vessels, known as “arterial transit artifact” (14). Reduced cardiac output, as seen frequently in elderly populations, leads to similar effects, e.g. in the vascular borderzone regions (15). The use of multi-TI ASL sequences aim to overcome this methodological shortcoming, but due to the longer scan times required, they are currently not recommended in daily clinical practice (16, 17).

Other parameters affecting ASL can be found in the online supplement.

ASL in neurodegenerative diseases

General considerations - coupling of brain perfusion and brain metabolism

Alzheimer Dementia (AD) is the most common type of dementia. According to the model of neurodegeneration proposed by Jack et al. (18), brain metabolic alterations precede structural abnormalities during cognitive decline in AD. This explains the considerable interest in the assessment of brain glucose metabolism based on FDG-PET (18F-2-fluoro-2-deoxy-D-glucose - positron emission tomography) in the work-up of dementia. This technique has identified typical patterns of metabolic alterations in various types of dementia. For example, AD is typically associated with hypometabolism in bilateral parietal and temporal regions sparing the occipital lobe, while dementia with

Lewy bodies also has bilateral parietal and temporal and additionally occipital hypometabolism (19). One disadvantage of FDG-PET is that the alterations in blood glucose metabolism are not specific for a given disease. This has led to the development of disease-specific tracers of amyloid- and tau-PET, which were recently introduced for clinical use. As a consequence, there is a need for an alternative technique, which might be used as a surrogate marker to replace FDG-PET in the work-up of dementia. ASL is a very promising alternative technique for two reasons. First, perfusion and metabolism are typically tightly coupled in the brain (20, 21). This perfusion-metabolism coupling implies that the known patterns of hypometabolism in FDG-PET in dementia can be transferred to patterns of hypoperfusion on ASL MRI. Correspondingly, there is a good correlation between brain perfusion measured using ASL (22-26) and brain metabolism measured by FDG PET (27-30), for example in the domain of MCI and AD. Second, structural MRI is routinely performed in many patients during the workup of cognitive decline. Adding an ASL sequence to the existing MR protocol is minimally demanding for the patient, and does not require additional radiation or use of contrast agents, is less costly and allows for the assessment of brain structure and perfusion in one imaging session. Moreover, if ASL could replace FDG PET, this would enable more disease-specific PET imaging with the newly available amyloid or tau tracers.

Normal aging

In order to be able to assess reductions in perfusion measured by ASL in cognitive decline, it is first necessary to understand the evolution of ASL

imaging appearances during normal aging. A study of 44 healthy participants from age 4 to 78, found the highest grey matter perfusion in children (97 ± 5 ml/100 g/minute) which had already deceased in adolescents (79 ± 3 ml/100 g/minute). After the age of around 20, grey matter perfusion remained rather constant at 58 ± 4 ml/100 g/minute until the age of around 80 (31). Another study of 38 elderly healthy individuals (mean age 82.2 ± 3.7) found variable patterns of decreased and increased perfusion (32). Restom and colleagues compared 15 healthy young adults around 25 years of age to 12 healthy elderly controls around 75 years old, and found a significantly lower CBF at rest in the elderly (33). Rusinek et al. focused on the hippocampus during normal aging from 26 to 92 years due to the particular interest of this structure in dementia, and found no statistically significant age or gender effect (34).

More recently, ASL was used in 148 consecutive control subjects and 65 MCI cases around 76 years of age (35). About half of the control participants developed subtle cognitive decline during follow-up. ASL imaging, performed at baseline, revealed decreased perfusion in the posterior cingulate cortex in those individuals who later developed subtle cognitive decline, indicating the predictive value of ASL for the earliest form of cognitive decline. Interestingly, the ASL pattern of those deteriorating controls was similar to MCI cases, indicating that these individuals were initially able to maintain an intact cognitive status through their cognitive reserve despite already present reductions in CBF.

Alzheimer's disease and mild cognitive impairment

Alzheimer's disease (AD) is associated with gray matter volume loss in the mesial temporal and parietal lobes. In earlier stages of the disease, such as mild cognitive impairment (MCI) or preclinical AD, atrophy can be minimal though metabolic imaging (FDG-PET) may already be abnormal (18, 36).

ASL studies in established AD have consistently shown a reduction in CBF (22-25, 30, 37, 38) in a posterior parietal distribution, including the precuneus, posterior cingulate, angular gyrus, and superior parietal gyrus (25). The ASL pattern is remarkably similar (Figure 4) to the pattern of the hypometabolism seen with FDG-PET (39) and both modalities have similar diagnostic performance (38). The information from ASL persists after correction for local gray matter atrophy, illustrating its independent diagnostic value, although uncorrected ASL maps may be preferred in a clinical setting to increase the effect-size. Similar patterns of hypoperfusion have been observed in subjects with MCI, and preliminary evidence suggests that abnormal perfusion in the precuneus can predict conversion to AD (40), though larger studies are required for confirmation.

Fronto-temporal lobar dementia, Lewy Body Dementia, and Vascular Dementia

Less is known about the potential of ASL in dementias other than AD. In subjects with fronto-temporal lobar dementia, Due et al. (30) found right frontal hypoperfusion in 21 patients, similar to FDG-PET, while perfusion in parietal regions and posterior cingulate was preserved relative to AD. These findings were confirmed in a study comparing AD and fronto-temporal lobar

dementia (41), with both ASL and FDG showing a clearly differentiating pattern in fronto-temporal lobar dementia compared to AD (Figure 4).

In dementia with Lewy bodies, Taylor et al (42) found posterior hypoperfusion in the posterior cingulate and higher-order visual association areas in 15 dementia with Lewy bodies patients; no comparison with AD was made. In the related Parkinson's Disease Dementia disorder, Le Heron et al. (43) found the pattern of posterior hypoperfusion to largely overlap with AD patients, hinting at a similar mechanism of neurodegeneration.

Vascular dementia by definition is caused by impaired cerebral perfusion and widespread decreases in CBF have been found especially in bilateral frontal and parietal areas in subjects with vascular dementia (44, 45) and subjects with confluent incidental white matter ischemic changes (46). The pattern overlaps even more with AD in post-stroke patients (47), though this may well be due to concomitant (unveiled) Alzheimer pathology. A related point to note here is the limited ability of ASL to measure white matter perfusion. Due to the low perfusion levels and long arterial arrival times in white matter, the SNR of the ASL signal is typically very low, and it is not possible to obtain reliable estimates of CBF unless the acquisition parameters are specifically optimized (48-50).

ASL in Cerebrovascular Disease

Early on, ASL techniques were recognized to be valuable for imaging brain ischemia. Indeed, following the National Institute of Neurological Disorders and Stroke (NINDS) trial (51) and the development of diffusion imaging, the potential of acquiring brain perfusion images without contrast was recognized. This allows perfusion imaging in patients with contraindications to IV contrast, such as renal failure, and simplifies the acquisition of quantitative CBF, which is challenging with contrast agent-based perfusion techniques, such as dynamic susceptibility contrast (DSC).

Initial reports of ASL imaging in stroke demonstrated proof-of-principle, but were limited by their inability to image the entire brain (52). Since the widespread use of whole-brain, high SNR ASL sequences, several studies have shown reasonable concordance of ASL with DSC measures of perfusion deficit, primarily time-based parameters such as the mean transit time and time-to-peak of the residue function (Tmax) (Figure 5). (53-56). Vessel-selective ASL has the additional advantage of being more sensitive to identify perfusion changes induced by collateral flow: (57) in stroke patients. Routine ASL can also show perfusion changes in Moyamoya patients (58). It has also been applied to cases where treatment was initiated on the basis of the presence of collateral flow (59).

The ability of ASL to measure severe hypoperfusion or determine perfusion in regions with prolonged arterial arrival times remains a critical issue for imaging patients with cerebrovascular disease. In these situations, there can be regions with a lack of ASL signal intensity in the ischemic lesion that

render reconstruction of summary maps difficult. However, for the detectability of stroke, ASL techniques have been shown to be at least equivalent to DSC techniques, and can be used for a mismatch approach with DWI images (54, 60). In our experience, it is particularly helpful when ASL shows normal perfusion or hyperperfusion (as is sometimes seen after vessel recanalization), since it eliminates the possibility of a diffusion-perfusion mismatch that would reflect tissue at-risk of infarction, thus directly affecting patient management.

In patients with known cerebrovascular disease, alternative ASL imaging strategies could be considered, including long-label long post-label delay single time-point ASL and multi-delay ASL. The former will mitigate the problem of slow flow not arriving at the tissue bed by the time of imaging, resulting in CBF underestimation. However, differences in the decay of the label when it is within the blood, with its longer T1 compared with tissue, can lead to misinterpretation, with adequate CBF that arrives later than expected appearing hyperintense. Multi-delay ASL, in which ASL images with several post-label delay times are acquired, offers the potential to measure both perfusion and arterial arrival time, and use the arrival time information to improve the accuracy of the CBF maps. This addresses some of the problems of long-label long-delay ASL, but at the expense of SNR per unit time. Practically, this means that multi-delay ASL scans will have reduced spatial resolution unless scan efficiency is improved or much longer imaging times are accepted. One promising approach to improve the time efficiency of multi-delay ASL is Hadamard encoding (61). Hadamard encoding is a method in

which blocks of labeling are mixed with blocks of non-labeling, with different permutations of the labeling and control blocks. This method enables reconstruction of images with different delay times in a more time-efficient manner, leading to higher SNR, particularly for transit time mapping. (61, 62).

ASL has also been applied to chronic cerebrovascular disease, including carotid stenosis and occlusion (14, 63, 64) and Moyamoya disease (58, 65-68). Such diseases are characterized by near normal CBF, but often striking abnormalities of arterial arrival time, since blood arrives at the parenchyma through alternative pathways. For this reason, many of these studies have availed themselves of multi-delay ASL approaches, to correct CBF values for arrival time, and to map transit time abnormalities directly (Figure 6). Given the relatively long delays, either the use of extremely long label and post-label delay times or multi-delay ASL is critical for a proper perfusion measurement in these diseases. This being said, even with state-of-the-art techniques, there are a few patients with very severe Moyamoya disease, in which ASL imaging of CBF is practically infeasible due to the extremely circuitious and delayed arrival time of the blood flow, due to loss of the magnetic label during the transit between the labeling region and the brain parenchyma.

ASL in AVM and fistula

One unexpected but useful clinical application of ASL imaging is the ability to identify lesions with arteriovenous shunting. Because >90% of water is extracted during the first pass through the capillaries, and because the mean

dwell time of water molecules once extracted from the vascular into the extravascular space is several minutes, most of the labeled water decays within the brain parenchyma, and does not reach the veins. This leads to the excellent depiction of parenchymal perfusion and the absence of vascular signal on most ASL scans. However, if the capillary bed is absent, as in the two most common shunting lesions of the CNS, the arteriovenous malformation (AVM) and dural arteriovenous fistula (AVF), ASL signal appears in venous structures (69). This can be quite striking, given the high blood volume of the veins (Figure 7).

While large AVM's and dural AVF's are not difficult to diagnose with routine anatomical MR imaging, small lesions or evolution of lesions following embolization therapies can be very challenging to identify. Le et al. demonstrated that identification of small (<2 cm) lesions was significantly improved if readers were allowed to view ASL in addition to conventional imaging (70). In fact, this may be more sensitive than conventional angiography, as venous signal on ASL has been seen in AVMs in the setting of intracranial hemorrhage where initial angiograms were negative, possibly due to mass effect. It has also been shown that identification of such lesions outside the brain, within the upper neck region, is also possible with ASL (71). Finally, shunting physiology has been identified in about 10% of developmental venous anomalies, suggesting that transitional lesions might be more common than is generally appreciated (72).

One challenge for ASL when using venous signal to identify shunt lesions is that conspicuity depends on the precise timing parameters (i.e., the labeling duration and the PLD. While the use of recommended parameters (10) appears fairly sensitive for detecting most lesions, it is possible that in either slow or fast shunting lesions, venous ASL signal could be suboptimal or missed. Therefore, there is interest in multi-delay ASL, in which images at different labeling duration and/or post label delay are acquired as part of a single acquisition. While these sequences were first developed for better CBF quantification, the ability to optimize the sensitivity for the detection of venous signal is also enhanced. However, spatial resolution is reduced compared with single-delay ASL for a given imaging duration, and thus any gains might be offset by this lower resolution. ASL-based multi-delay MR angiographic sequences have also been developed, focusing more on direct vessel visualization (73). As such, these latter sequences would compete more directly with conventional angiography, with comparable temporal resolution without the associated risks.

ASL in Epilepsy

The main interest of ASL in the context of epilepsy is to locate a potential epileptogenic focus. ASL might further be helpful in the differential diagnosis for example in assessing for a stroke in the acute stage. During the acute peri-ictal period, the CBF is typically increased due to pathologic neuronal activity (74), while in the chronic inter-ictal period, CBF is typically reduced as the epileptogenic region typically is less functional and active as compared to

the normal brain tissue (75-79).

Nuclear medicine techniques such as ictal and inter-ictal SPECT and PET are often performed to detect metabolic changes related to epileptic activity. Since standard structural MR imaging is routinely performed, ASL might be of interest as an additional functional marker of cerebral perfusion with minimal additional effort. Hypoperfusion on ASL corresponds to hypoperfusion on interictal PET and electrophysiological data (75, 76, 80), indicating the potential use of ASL for epileptic focus localization (*Figure 8*).

ASL in neoplasms

Hemodynamic changes are present in many CNS neoplasms, and in general, CBF and cerebral blood volume (CBV) increase with tumor grade. Historically, much of our MR-based knowledge about these hemodynamic changes has been gained from DSC and dynamic contrast enhancement (DCE) imaging (81-87). This has had two main consequences: (1) most literature has focused on relative CBV changes, because the DSC measurement of CBV is more straightforward compared with CBF, and (2) most of our data is of relatively poor spatial resolution and prone to artifacts, since the rapid passage of the intravascularly-confined tracer necessitates rapid, sometimes suboptimal, imaging. ASL cannot measure relative CBV; instead, CBF measurements are more straightforward. While CBV and CBF are related via the Grubb's law ($CBV = CBF^{0.38}$) in normal tissue (88), it is likely that this relationship is altered in tumors, which may form abnormal blood vessels that alter the CBV/CBF

ratio. Also, since there is no requirement to accurately track a rapid intravascular bolus of contrast, the ASL experiment is more flexible, such that SNR, spatial resolution, amount of tolerable image distortion, and imaging time may be traded off against one another. Lastly, since water has high permeability in the normal and neoplastic tissue, there is no need with ASL (unlike DSC) to employ complicated leakage-correction algorithms to obtain quantitative results.

Primary CNS Neoplasms

GBM is the most common high-grade CNS tumor in adults, and is associated with high metabolism and CBF (Figure 9). Initial reports demonstrated that ASL and DSC show largely concordant results in terms of identifying this tumor, and distinguishing it from contrast-enhancing mimics (89-92). Higher CBF in GBM correlates with genetic markers (such as epidermal growth factor receptor) and is associated with shorter progression free survival time (93). Lower grade tumors typically demonstrate lower CBF. CBF changes may portent transformation to a more aggressive phenotype. In fact, some have suggested that CBF quantification provides a better estimate of event-free survival for a wide range of gliomas than does a histological grading scale (94). One exception to this rule of increasing CBF and tumor grade is oligodendroglioma, a grade 2 tumor that often demonstrates increased CBF.

Secondary CNS lesions

Most metastatic brain lesions show similar or lower glucose uptake and CBF compared with gray matter. However, several metastatic lesions demonstrate

increased CBF, and share the feature of high vascularity. These include renal cell carcinoma (95), angiosarcoma, hemangioblastoma (96), and melanoma, and in these cases, ASL may be helpful (Figure 10).

Assessing treatment response

The quantitative nature of ASL has enabled studies of CBF changes over time or with treatment, to assess its impact on prognosis and outcome. A particularly important and challenging distinction to make is between radiation necrosis and recurrent tumor in patients with new or increasing contrast enhancement. Since radiation necrosis is associated typically with reduced CBF and most recurrent tumors demonstrate increased CBF, perfusion imaging may be helpful to distinguish the two entities. DSC and MR spectroscopy have also been used for this distinction, with some success (97-99). ASL is likely to improve upon DSC perfusion measures, given its better imaging performance around resection cavities (where blood products can affect DSC results). It is also less sensitive to the presence of surrounding large vessels, which can make it challenging to quantify CBF in the actual lesion (Figure 11).

Using clinical and imaging endpoints, Oszunar et al. (100) suggested that ASL is superior to FDG PET and DSC for distinguishing tumor recurrence from radiation necrosis in gliomas, with a sensitivity of 94%. In the early time period following resection (< 4 wks), where any contrast enhancement is probably due to pseudo-progression, again ASL appeared more useful than DSC (101). Another technique that can evaluate both initial presentation and treatment

changes in tumors is DCE imaging, in which the rate of contrast agent leakage is estimated.

ASL in psychiatric and other neurologic disorders

An increasing number of investigations have assessed ASL in various psychiatric and neurologic diseases.

Depression

In a study of 25 medication-naive adolescents with major depressive disorder, Ho et al., found a complex pattern of hypoperfusion in frontal, limbic, paralimbic, and cingulate yet hyperperfusion within the subcallosal cingulate, putamen, and fusiform gyrus (102). The authors conclude that adolescents with major depressive disorder differ in their baseline perfusion in executive, affective, and motor networks. Several studies assessed adults with depression and found reduced CBF in the default mode network (103) (a brain network initially described based on CBF maps (104) that is consistently found in resting fMRI studies (105)) as well as bilateral subgenual anterior cingulate cortex, left prefrontal dorso-median cortex, and left subcortical areas (putamen, pallidum and amygdala) (106). Lui et al. further subdivided patients with refractory depressive disorder from patients with non-refractory depressive disorder (107). Non-refractory depressive disorder subjects versus controls had reduced CBF in the left prefrontal cortex and increased CBF mainly in the limbic-striatal areas. Conversely, refractory depressive disorder subjects had decreased CBF predominantly in the bilateral frontal and

bilateral thalamic regions. The direct comparison of the two depressive disorder groups further revealed higher CBF mainly in the limbic-striatal areas. Finally, late-life depression is associated with increased white matter CBF yet conserved grey matter CBF (108). In conclusion, these results indicate that different subtypes of depression are associated with specific patterns of CBF alterations, which furthermore change over the lifespan.

Psychosis

Patients with schizophrenia compared to controls had a pattern of increased CBF in left putamen/superior corona radiata and right middle temporal gyrus yet decreased CBF in bilateral precuneus and middle frontal gyrus (109). Moreover, a sub-division into patients according to symptomatology revealed an association of negative symptoms (including difficulties in thinking or coming up with ideas, decreased ability to start initiate tasks, lowered levels of motivation or drive, lack of interest in other people) with reduced CBF in bilateral superior temporal gyrus, cingulate gyrus, and left middle frontal gyrus, and an association of positive symptoms (including delusions, hallucinations, disorganized speech or behavior) with increased CBF in cingulate gyrus and superior frontal gyrus and decreased CBF in precentral gyrus/middle frontal gyrus. Astudy by Ota et al. found a different pattern of reduced relative CBF in the left prefrontal and bilateral occipital cortices compared to the healthy volunteers (110). Finally, Kindler et al. observed decreased mean CBF in the frontal and temporal regions and significantly increased default mode network connectivity in the precuneus in schizophrenia patients. Currently it is impossible to disentangle whether these

observed differences in ASL based alterations in CBF in schizophrenia patients are due to different stages and subtypes of the disease, methodological, or a combination of both.

Posttraumatic stress disorder

Posttraumatic stress disorder (PTSD) has attracted considerable interest in recent years. Schuff et al. assessed 17 male veterans with PTSD and observed increased relative CBF in primarily right parietal and superior temporal cortices (111). Li et al. implemented a more complex setup in veterans nearly 20 years after the 1991 Gulf War, contrasting baseline ASL with a physostigmine challenge (112). Physostigmine significantly decreased hippocampal relative CBF in controls and veterans with syndrome 1 (impaired cognition), yet significantly increased hippocampal relative CBF in veterans with syndrome 2 (confusion-ataxia) and 3 (central neuropathic pain), suggesting that ASL might differentiate subtypes of PTSD types.

Mild traumatic brain injury

Mild traumatic brain injury (MTBI) is another entity that has attracted considerable interest, notably related to the discussion of brain alterations in professional football and soccer players. Conventional MRI sequences are not sensitive enough to detect structural brain changes, and consequently an increasing number of investigations used advanced imaging techniques such as ASL or diffusion weighted imaging (113). In 2009, Ge et al. demonstrated reduced CBF in bilateral thalamus in patients with MTBI (114). Later on, the same group extended these findings by combining ASL to assess CBF and

diffusion tensor (DTI) and diffusion kurtosis (DKI) imaging to assess white matter, again detecting substantial alterations in both perfusion and white matter integrity in MTBI patients focusing on the thalamus (113). Interestingly these alterations persisted more than 9 months after injury. Doshi et al. assessed the acute stage of MTBI and found increased in regional CBF in the left striatum, and in frontal and occipital lobes (115). Finally, Wang et al. investigated pediatric MTBI and found reduced CBF in bilateral frontotemporal regions (116). In summary, these results indicate that ASL might be a sensitive marker to assess MTBI-related alterations in the brain, which are not detectable by conventional MRI techniques. The discrepancies between these studies in turn also implies the need for strict standardization of both data acquisition and data analysis.

Pain and migraine

Owen et al. investigated healthy volunteers during painful thermal stimulation and observed bilateral CBF changes including the insula, secondary somatosensory, and cingulate cortices, as well as the supplementary motor area, in an attempt to quantify pain-induced perfusion alterations in the brain (117). A similar approach by Maleki et al. found alterations in relative CBF in somatosensory cortex, anterior cingulate cortex, anterior insula, hippocampus, amygdala, thalamus, and precuneus. Taken together, these studies suggest that ASL might be used as an operator-independent marker in subjective pain syndromes. Accordingly, Liu et al. observed in patients with postherpetic neuralgia, a pattern of increased CBF in left striatum, right thalamus, left primary somatosensory cortex, left insula, left amygdala, left

primary somatomotor cortex, and left inferior parietal lobule yet decreases CBF in the frontal cortex (118).

Migraine is of particular interest with respect to ASL imaging. Although controversial, it is thought that migraine attacks might involve vascular dysregulation. Correspondingly, mapping the brain CBF by ASL might reveal insights into the pathophysiology of migraine. Kato et al. performed ASL imaging in a patient during a migraine attack, after treatment with a triptan and in the attack-free period (119). During the migraine attack, CBF was reduced in bilateral median thalamic areas including hypothalamus and increased in the frontal cortex as compared to baseline. 30 minutes after treatment initiation, CBF perfusion improved in thalamus and hypothalamus. A case series sby Pollock et al. demonstrated regional cerebral hyperperfusion in 3/ 11 patients during a headache episode that corresponded to previous aura symptoms (120). While these pilot studies demonstrated interesting preliminary findings, larger scale studies are clearly needed to investigate whether ASL might contribute to a better understanding of the pathophysiology of pain, notably a potential vascular component of migraine.

Novel extensions of ASL

Super-selective ASL to map vascular territories (aka selective territory mapping)

Contrary to contrast-enhanced CT perfusion or DSC, ASL provides the opportunity to selectively label vascular territories, such as left carotid, right carotid and vertebrobasilar territories (121, 122) or even their more distal branches. This can be of interest from a scientific perspective, for example, to

assess the impact of vascular variants of the circle of Willis on perfusion of the brain tissue, such as caudate and lenticular nucleus and thalamus (123). More importantly, territorial ASL might have clinical value, e.g., to determine whether multiple acute vascular lesions are in the same vascular territory as argument for distant cardio-embolic events in several vascular territories versus local stenotic origin for a single vascular territory or for neurosurgical planning of e.g. aneurysm clipping or tumor resection.

Cerebrovascular Reserve Imaging

The ability of an organ to adapt to a physiological challenge, particularly one that stresses its limits, can be measured using reserve studies. Such imaging may unmask deficits that are not apparent on routine images. Myocardial stress-rest imaging following either exercise or pharmaceutical vasodilatory challenge has been a mainstay of cardiac imaging for decades. A similar cerebrovascular “stress test” can be performed, using either physiological (i.e., CO_2 inhalation or breath-hold) and pharmaceutical vasodilation. In particular, acetazolamide, a carbonic anhydrase inhibitor, causes 20-50% CBF increase in normal subjects. However, patients in whom the cerebrovasculature is already maximally dilated to maintain baseline CBF may not be able to augment their CBF further in response to an acetazolamide challenge. In fact, those with very severe disease may demonstrate reduced CBF in response to challenge, a phenomenon known as cerebrovascular steal.

Limited data using non-MRI techniques, including transcranial Doppler, SPECT, and PET suggest that demonstration of poor reserve is an important risk factor for subsequent cerebrovascular events (124). Given its non-invasive nature, ASL is an ideal method to image CBF changes in response to a challenge (14, 125). Since these patients may have large artery stenosis or occlusion, the use of multi-delay ASL to quantify both arrival time and CBF is recommended. An example of reserve imaging with multi-delay ASL in a patient with Moyamoya disease with cerebrovascular steal of the bilateral anterior circulation is shown in Figure 12.

Functional MRI and ASL

Functional MRI studies generally rely on the blood oxygen level-dependent (BOLD) effect (126) and the neurovascular coupling (127). Because fMRI does not directly measure neuronal activation but the indirect vascular response, alterations of the neurovascular coupling might influence the resulting fMRI BOLD signal, for example already in normal aging (33, 128). The combination of ASL and fMRI might disentangle vascular and neuronal contributions of the BOLD response (128).

Moreover it is possible to use the time-series of the ASL raw data to calculate fMRI activation maps (129) or resting-state functional connectivity networks known from fMRI (105). Although the quality of these ASL based results is generally below that of classic EPI BOLD fMRI, this might be interesting from a clinical perspective as ASL can be used to calculate relative CBF maps and resting-state functional connectivity networks of a reasonable quality without

additional cost or scanning time which is particularly helpful in elderly patients (Figure 13).

Conclusions

Although ASL has been around for over two decades, it only recently began to make the transition from a research tool to clinical use due increasing awareness of radiologists and clinicians of its capability and technical improvements that have made this approach more reliable and available as product sequences on MRI platforms. For many diseases, including dementia, vascular diseases, neoplasms, and various psychiatric diseases, ASL provides additional and complimentary information to that available from structural MRI imaging. Current methodological developments aim to increase the robustness and decrease inter-scanner variability of CBF estimation.

Online supplement

Quantification of CBF and local alterations in CBF estimation

A number of investigations directly compared CBF estimation in ASL to 15O H2O PET as reference standard (16, 130, 131) or combined PET-MRI technology (132, 133). Overall, these studies showed good correlations between CBF estimation in ASL and PET. Furthermore, most studies showed a systematic bias of relative CBF estimation in ASL. In addition, the

placement of the imaging slab substantially changes the relative CBF estimation in ASL and the correlation with water PET (134) indicating the need for rigorous standardization of image acquisition. Moreover, the direct comparison between two different ASL sequences (135) demonstrated a good global correspondence between the relative CBF estimated by both techniques but also pointed to systematic local differences between the results, even if acquired with both sequences during the same session. Note that differences in the calibration method used explained most of the results in this case. It is likely that different ASL sequences on different MRI machines with different hardware will show even larger differences in the estimated relative CBF maps. This implies that individual ASL sequences might have variations in local sensitivity, which in turn highlights the need for strict standardization of image acquisition and calibration of each ASL sequence, e.g. using flow phantoms. This is of particular interest in neurodegenerative diseases, as disease-related alterations in relative CBF, notably at early stages of the disease, are well in the range of normal variability between different ASL sequences even when these sequences (135) are performed with recently recommended protocols (10).

Partial volume correction

Another potential issue with ASL is the relatively low spatial resolution typically used (on the order of a few millimeters in each direction), which makes it nearly impossible to obtain any relative CBF measure located uniquely within the cortical ribbon (136). Due to the large difference in perfusion values between gray and white matter (in a ratio of 3:1), even a

small amount of white matter within a voxel located primarily within gray matter will lead to an artificially low perfusion value. For this reason, a series of post-processing techniques have been developed, using the assumption that the relative CBF only varies slowly within the gray matter (and white matter) to separate the contributions from each tissue type to the perfusion maps (136). This method might be particularly important when focusing on statistical differences between patients presenting with gray matter atrophy, enabling reduced perfusion to be differentiated from an increased proportion of white matter relative CBF in a thinning cortical ribbon (though one could argue from a pragmatic viewpoint that it does not matter why perfusion is abnormally low).

Reproducibility, Inter-individual Variability and SNR

For many years, developments of ASL focused on methodological improvements and did not investigate the important issue of intra- and inter-subject reproducibility. One of the first large-scale reproducibility studies was published in 2010, based on the QUASAR sequence (137). The mean gray matter CBF was determined to be 47.4±7.5 ml/100 g/min in that study, with a standard deviation between the different sites SDs = 1.8 (CI: 1.0–3.3) ml/100 g/min, a between-subject standard variation of 5.5 (CI: 5.0–6.2) ml/100 g/min and a within-subject standard deviation of 4.7 (CI: 4.5–5.0) ml/100 g/min with a corresponding repeatability of 13.0 ml/100 g/min. Such results - based on more than 280 subjects - showed that using a single sequence in different research centers was possible, and demonstrated that the reproducibility

achieved by ASL was comparable to equivalent nuclear medicine methods (137).

Note that for this study all data were acquired on identical 3T scanners from a single manufacturer. Since then, numerous other studies have been published, comparing different sequences on a single manufacturer (138), near identical sequences on different manufacturers (139), and combinations in between. The general results confirm the same level of reproducibility, within and between subject standard deviations as originally found in the QUASAR reproducibility study (137). Potential site-specific variations in gray matter CBF values might actually be problematic, and current research is focusing on eliminating such differences to avoid bias in future multicenter trials (10).

1.5T versus 3T

Since ASL is a low SNR technique, it benefits substantially from any possible increase in SNR. SNR increases approximately linearly with field strength, and therefore 3T is expected to increase SNR by a factor of two relative to 1.5T (4). In addition, T1 also increases with field strength, resulting in a slower disappearance of the labeled blood at 3T (T1blood = 1.65s) than at 1.5T (T1blood=1.35s). Both effects will act together to increase SNR, and the ASL white paper therefore recommended the use of higher field strengths for ASL (10).

2D versus 3D acquisition schemes

The most widely used image acquisition scheme for ASL is EPI, which is a multi-slice 2D technique. The intrinsic SNR advantage of 3D acquisition schemes renders them an attractive alternative for the imaging module of ASL sequences. Various approaches have been implemented, including 3D GRASE (140), 3D spiral FSE (9) and 3D EPI (141). Although 3D image readout methods have some challenges regarding image acquisition speed and resolution, overall, they are advantageous for ASL, for several reasons. In addition to the intrinsic SNR increase gained from exciting the entire volume with each read-out, they have the additional advantage that it is possible to define a precise time at which the whole volume is imaged. This contrasts with 2D techniques such as multi-slice EPI, where each brain slice is acquired at a different time, and consequently has a different PLD. As well as simplifying CBF quantification and avoiding any potential saturation of inflowing blood by previous slice excitation pulses, a single TI/PLD enables optimal background suppression to be achieved over the whole imaging slab, therefore providing higher SNR and improved data quality for clinical use.

Variation of ASL CBF due to caffeine and other vasoactive substances

Vasoactive substances are frequently prescribed notably in the elderly, and may alter CBF. It may be less appreciated that even substances such as caffeine, which are widely distributed in beverages such as cola or coffee, significantly reduce the CBF estimated in ASL imaging, by about 20% in young adults (142) and even more in elderly controls (by approximately 23-25%) and mild cognitive impairment (MCI) (~30%) (143, 144). Disease-related alterations in relative CBF, for example in dementia, are considerably smaller

than caffeine-induced reduction of global CBF. Consequently, vasoactive substances must be considered as a potential confound for quantitative analyses of relative CBF, and compensation strategies such as normalizing with respect to whole brain average relative CBF might be worth considering, depending on the clinical context. These observations indicate that in particular in conditions in which relatively subtle alterations of relative CBF are expected, notably dementia or psychiatric diseases, patients should be asked to refrain from caffeine ingestion 4-6 h prior to MR imaging.

Decreased cardiac output / alterations in hematocrit

Decreased cardiac output might lead to delayed arrival of the labeled blood, which might be misinterpreted as reduced perfusion. Therefore, care needs to be taken when scanning patients with potential cardiac issues, as the entire circulation system might be affected. Other systemic alterations might directly affect brain perfusion, such as a change in hematocrit. Indeed, the normal physiological response to a reduced amount of oxygen carrying capacity will be to increase blood flow systemically throughout the body, and in particular to the most important organs, such as the brain. The problem for ASL is that a reduced hematocrit will also be accompanied by an increase in blood relaxation time T1b (145, 146), leading to a potential overestimation of perfusion measured by ASL, as the label will disappear at a slower rate than assumed. Note that these issues are particularly relevant in neonates (147) and in patients with erythrocyte-related diseases, such as Sickle Cell Disease (148).

FIGURE 1

ASL labeling schemes: (a) in PASL, an inversion slab is placed proximal to the imaging volume to label blood in the arterial feeding vessels supplying the brain. The pulse is short (~10ms) and all the blood is inverted simultaneously; (b) in pCASL, the inflowing arterial blood is continuously inverted as it flows through the labeling plane, via a process known as flow-induced adiabatic inversion. The pCASL labeling pulse train is typically applied for a period of ~1-2s.

FIGURE 2

Differences in labeling degree of ASL bolus for PASL (left column) and pCASL (right column). The top row shows the temporal profile of the bolus (1=fully inverted; 0=fully relaxed). Since the PASL inversion slab is inverted at a single point in time (t=0 on this graph), all the inflowing arterial blood undergoes the same amount of T1 recovery at all time points after this. In pCASL, blood is labeled as it flows through the inversion plane and recovers en route to the imaging volume. A-D shows the degree of labeling remaining at several time points after the (start of) labeling (t=0): A t=0; B t = arterial arrival time (ATT); C t = bolus duration (τ); D t = ATT + τ. Color scale represents the range from fully inverted (red) to fully relaxed (blue). It can be seen that the pCASL labeling process produces a bolus with a higher overall degree of inversion than PASL, resulting in a higher intrinsic SNR for pCASL.

Figure 3

Example of an underestimation of relCBF in ASL due to a proximal vessel stenosis: The estimated relative CBF based on DSC perfusion is within normal limits (A). In contrast, the relative CBF estimated using a standard single TI ASL sequence demonstrates a marked reduction in the left anterior and middle cerebral artery territories (B). The origin of this discrepancy is the increased perfusion delay, illustrated in the DSC-derived delay map (C), which exactly matches the altered perfusion in ASL, due to the presence of a high-grade stenosis of the left internal carotid artery (time of flight, D). The underlying principle is explained in E. The normal perfusion time-series of DSC imaging (solid black line) is shifted to the right due to the presence of a proximal vessel stenosis and slower collateral flow (dotted line). As DSC imaging acquires an entire time-series, this shift in the bolus arrival simply cases a shift of the estimated curve, and the relative CBF can be accurately estimated in DSC. In contrast, a single TI ASL sequence with a standard TI (indicated by the vertical line) will under-estimate the true perfusion simply because it is too early with respect to the peak of the perfusion curve.

FIGURE 4 Examples of dementia.

Transverse FDG and ASL images of a healthy individual (first row, male, age 57, mini mental state examination 30), patient with AD (second row, male, age 52, MMSE 19), and patient with fronto-temporal lobar dementia (third row, female, age 53, MMSE 26). Functional images show predominant prefrontal abnormalities in FTD and parietal abnormalities in AD. 'Red color' reflects normal metabolism and perfusion.

FIGURE 5

50 year-old woman presenting with stroke with 14 hrs of right hemiparesis and aphasia, national institute of health stroke scale (NIHSS) of 9 at the time of imaging. Patient later found to have extracranial left internal carotid artery dissection. (A) demonstrates irreversibly damaged tissue on DWI within the left caudate and putamen. Using a multidelay ASL sequence capable of acquiring both (B) CBF and (C) arterial transit time images, a larger region of perfusion abnormality is identified. (D) The region of perfusion abnormality (time to the maximum of the residue function, Tmax) on conventional dynamic susceptibility contrast images is concordant with the findings on the ASL images.

Figure 6

Example of multi-delay ASL imaging. A fixed labeling duration of 2000 ms is used, but on subsequent images, different post-label delays (PLDs) ranging from 700 to 3000 ms are employed, yielding ASL difference (control – label) images as shown in (a). From this data, and the use of general kinetic modeling, one can simultaneously measure (b) an arrival-time corrected CBF and (c) the arterial arrival time itself. In this patient, there is near symmetric CBF but clear arterial arrival delay in the right hemisphere, as shown by the higher values on the arrival time map.

FIGURE 7

51 year-old man with exertional headaches, imaged at 1.5T with an AV fistula. (A) T2 images demonstrate very subtle flow voids in the inferior frontal lobe (arrows). (B) ASL images demonstrate very bright linear signal in the region of the right inferior frontal lobe, which extends to the right cavernous sinus, indicative of an arteriovenous shunt lesion. (C) Collapsed and (D) source MR angiographic images confirm the presence of an ethmoid dural fistula, which was recognized only after the observation of the abnormal ASL signal within the venous structures draining the fistula. This case also demonstrates that while 3T is preferable to 1.5T, relevant clinical information can be obtained with ASL at 1.5T.

FIGURE 8

Comparison of ASL MRI and 18FDGPET in epilepsy. Each vertical column represents a single patient's imaging studies. A: preoperative axial T1 weighted MRI. B: raw 18FDG PET scan images. C: raw pASL CBF maps. D: image fusion of T1MRI and 18FDG PET. E: image fusion of T1MRI and pASL. Arrows indicate regions of focal cortical dysplasia that are epileptogenic.

Reprinted with permission from (80).

FIGURE 9

78 year old man with unresectable anaplastic astrocytoma (WHO Grade III), seen on (A) post-contrast T1-weighted and (B) FLAIR images. (C) ASL demonstrates increased CBF in the region of the tumor. (D) Increased CBV is also visible on bolus dynamic susceptibility contrast (DSC) imaging (black arrow), though it is more difficult to appreciate due to the extensive number of arterial and venous vessels that surround the tumor. The findings of high CBF are characteristic of high-grade (Grades III and IV) glial neoplasms.

FIGURE 10

T2 (A), post-contrast T1 (B), and ASL (C) images in a 40 yo man with von Hippel Lindau disease and multiple hemangioblastomas, status post multiple prior surgeries. Arrows point out the extremely high CBF measured with ASL even in very small lesions.

FIGURE 11

57 yo man with lung cancer brain metastasis, 15 months status post resection, radiation, and chemotherapy. (A) Axial T1Gd shows a new enhancing lesion with (B) axial FLAIR demonstrating extensive vasogenic edema in the region of the resection cavity. (C) ASL demonstrates no increase in CBF in this region, similar to findings on (D) FDG PET. These findings were considered to represent radiation necrosis and the patient is being followed serially rather than with re-resection.

FIGURE 12

29 year-old woman with bilateral Moyamoya disease. Both FLAIR (A) and diffusion-weighted images (B) show evidence of prior infarcts in the deep white matter on the left side. Multi-delay ASL images acquired at baseline demonstrates normal CBF in the bilateral anterior circulation (C). However, imaging 10 min following 1 g of IV acetazolamide (D) demonstrates the expected CBF increase in the posterior circulation, but marked reduction in CBF in both anterior circulations, compatible with cerebrovascular steal. This finding has been associated with a high risk of subsequent cerebrovascular events and prompted bilateral direct superficial temporal artery-middle cerebral artery bypass.

FIGURE 13

Functional connectivity analysis on the ASL raw-data in 154 healthy elderly controls and 66 mild cognitive impairment (MCI) cases. Note that for illustrative purposes, the raw ASL data were directly analyzed using tensorial independent component in FSL (www.fmrib.ox.ac.uk/fsl/). The spatial representation of one of the independent components is illustrated in A. The on-off labeling pattern of the raw ASL data is clearly visible in the corresponding temporal representation in B. Adding the known prior knowledge of the on-off time-course could further improve the resulting functional connectivity networks.

References

1. Detre JA, Leigh JS, Williams DS et al. Perfusion imaging. Magn Reson Med 1992; 23(1):-37-45.
2. Williams DS, Detre JA, Leigh JS et al. Magnetic resonance imaging of perfusion using spin inversion of arterial water. Proc Natl Acad Sci U S A 1992; 89(1):-212-216.
3. Roberts DA, Detre JA, Bolinger L et al. Quantitative magnetic resonance imaging of human brain perfusion at 1.5 T using steady-state inversion of arterial water. Proc Natl Acad Sci U S A 1994; 91(1):-33-37.
4. Golay X, & Petersen ET. Arterial spin labeling: benefits and pitfalls of high magnetic field. Neuroimaging Clin N Am 2006; 16(2):-259-68, x.
5. Kety SS, & Schmidt CF. THE NITROUS OXIDE METHOD FOR THE QUANTITATIVE DETERMINATION OF CEREBRAL BLOOD FLOW IN MAN: THEORY, PROCEDURE AND NORMAL VALUES. J Clin Invest 1948; 27(4):-476-483.
6. Kety SS, & Schmidt CF. The determination of cerebral blood flow in man by use of nitrous oxide in low concentrations. Am J Physiol 1945; 14353-66.
7. Vidorreta M, Wang Z, Rodriguez I et al. Comparison of 2D and 3D single-shot ASL perfusion fMRI sequences. Neuroimage 2013; 66662-671.
8. Vidorreta M, Balteau E, Wang Z et al. Evaluation of segmented 3D acquisition schemes for whole-brain high-resolution arterial spin labeling at 3 T. NMR Biomed 2014; 27(11):-1387-1396.
9. Dai W, Garcia D, de Bazelaire C et al. Continuous flow-driven inversion

for arterial spin labeling using pulsed radio frequency and gradient fields. Magn Reson Med 2008; 60(6):-1488-1497.

10. Alsop DC, Detre JA, Golay X et al. Recommended implementation of arterial spin-labeled perfusion MRI for clinical applications: A consensus of the ISMRM perfusion study group and the European consortium for ASL in dementia. Magn Reson Med 2014;
11. Alsop DC, & Detre JA. Reduced transit-time sensitivity in noninvasive magnetic resonance imaging of human cerebral blood flow. J Cereb Blood Flow Metab 1996; 16(6):-1236-1249.
12. Wong EC, Buxton RB, & Frank LR. Quantitative imaging of perfusion using a single subtraction (QUIPSS and QUIPSS II). Magn Reson Med 1998; 39(5):-702-708.
13. Deibler AR, Pollock JM, Kraft RA et al. Arterial spin-labeling in routine clinical practice, part 2: hypoperfusion patterns. AJNR Am J Neuroradiol 2008; 29(7):-1235-1241.
14. Detre JA, Samuels OB, Alsop DC et al. Noninvasive magnetic resonance imaging evaluation of cerebral blood flow with acetazolamide challenge in patients with cerebrovascular stenosis. J Magn Reson Imaging 1999; 10(5):-870-875.
15. Zaharchuk G, Bammer R, Straka M et al. Arterial spin-label imaging in patients with normal bolus perfusion-weighted MR imaging findings: pilot identification of the borderzone sign. Radiology 2009; 252(3):-797-807.
16. Bokkers RP, Bremmer JP, van Berckel BN et al. Arterial spin labeling perfusion MRI at multiple delay times: a correlative study with H(2)(15)O positron emission tomography in patients with symptomatic carotid artery

occlusion. J Cereb Blood Flow Metab 2010; 30(1):-222-229.

17. Petersen ET, Lim T, & Golay X. Model-free arterial spin labeling quantification approach for perfusion MRI. Magn Reson Med 2006; 55(2):-219-232.
18. Jack CRJ, Knopman DS, Jagust WJ et al. Hypothetical model of dynamic biomarkers of the Alzheimer's pathological cascade. Lancet Neurol 2010; 9(1):-119-128.
19. Brown RK, Bohnen NI, Wong KK et al. Brain PET in suspected dementia: patterns of altered FDG metabolism. Radiographics 2014; 34(3):-684-701.
20. Buxton RB, & Frank LR. A model for the coupling between cerebral blood flow and oxygen metabolism during neural stimulation. J Cereb Blood Flow Metab 1997; 17(1):-64-72.
21. Aubert A, & Costalat R. A model of the coupling between brain electrical activity, metabolism, and hemodynamics: application to the interpretation of functional neuroimaging. Neuroimage 2002; 17(3):-1162-1181.
22. Yoshiura T, Hiwatashi A, Noguchi T et al. Arterial spin labelling at 3-T MR imaging for detection of individuals with Alzheimer's disease. Eur Radiol 2009; 19(12):-2819-2825.
23. Yoshiura T, Hiwatashi A, Yamashita K et al. Simultaneous Measurement of Arterial Transit Time, Arterial Blood Volume, and Cerebral Blood Flow Using Arterial Spin-Labeling in Patients with Alzheimer Disease. AJNR Am J Neuroradiol 2009; 30(7):-1388-1393.
24. Dai W, Lopez OL, Carmichael OT et al. Mild cognitive impairment and alzheimer disease: patterns of altered cerebral blood flow at MR

imaging. Radiology 2009; 250(3):-856-866.

25. Binnewijzend MA, Kuijer JP, Benedictus MR et al. Cerebral blood flow measured with 3D pseudocontinuous arterial spin-labeling MR imaging in Alzheimer disease and mild cognitive impairment: a marker for disease severity. Radiology 2013; 267(1):-221-230.
26. Wolk DA, & Detre JA. Arterial spin labeling MRI: an emerging biomarker for Alzheimer's disease and other neurodegenerative conditions. Curr Opin Neurol 2012; 25(4):-421-428.
27. Bozoki AC, Korolev IO, Davis NC et al. Disruption of limbic white matter pathways in mild cognitive impairment and Alzheimer's disease: a DTI/FDG-PET study. Hum Brain Mapp 2012; 33(8):-1792-1802.
28. Pagani M, Dessi B, Morbelli S et al. MCI patients declining and not-declining at mid-term follow-up: FDG-PET findings. Curr Alzheimer Res 2010; 7(4):-287-294.
29. Herholz K, Salmon E, Perani D et al. Discrimination between Alzheimer dementia and controls by automated analysis of multicenter FDG PET. Neuroimage 2002; 17(1):-302-316.
30. Du AT, Jahng GH, Hayasaka S et al. Hypoperfusion in frontotemporal dementia and Alzheimer disease by arterial spin labeling MRI. Neurology 2006; 67(7):-1215-1220.
31. Biagi L, Abbruzzese A, Bianchi MC et al. Age dependence of cerebral perfusion assessed by magnetic resonance continuous arterial spin labeling. J Magn Reson Imaging 2007; 25(4):-696-702.
32. Lee C, Lopez OL, Becker JT et al. Imaging cerebral blood flow in the cognitively normal aging brain with arterial spin labeling: implications for

imaging of neurodegenerative disease. J Neuroimaging 2009; 19(4):-344-352.

33. Restom K, Bangen KJ, Bondi MW et al. Cerebral blood flow and BOLD responses to a memory encoding task: a comparison between healthy young and elderly adults. Neuroimage 2007; 37(2):-430-439.
34. Rusinek H, Brys M, Glodzik L et al. Hippocampal blood flow in normal aging measured with arterial spin labeling at 3T. Magn Reson Med 2011; 65(1):-128-137.
35. Xekardaki A, Rodriguez C, Montandon ML et al. Arterial Spin Labeling May Contribute to the Prediction of Cognitive Deterioration in Healthy Elderly Individuals. Radiology 2015; 274(2):-490-499.
36. Jack CRJ, Knopman DS, Jagust WJ et al. Tracking pathophysiological processes in Alzheimer's disease: an updated hypothetical model of dynamic biomarkers. Lancet Neurol 2013; 12(2):-207-216.
37. Alsop DC, Detre JA, & Grossman M. Assessment of cerebral blood flow in Alzheimer's disease by spin-labeled magnetic resonance imaging. Ann Neurol 2000; 47(1):-93-100.
38. Musiek ES, Chen Y, Korczykowski M et al. Direct comparison of fluorodeoxyglucose positron emission tomography and arterial spin labeling magnetic resonance imaging in Alzheimer's disease. Alzheimers Dement 2012; 8(1):-51-59.
39. Chen Y, Wolk DA, Reddin JS et al. Voxel-level comparison of arterial spin-labeled perfusion MRI and FDG-PET in Alzheimer disease. Neurology 2011; 77(22):-1977-1985.
40. Chao LL, Buckley ST, Kornak J et al. ASL perfusion MRI predicts

cognitive decline and conversion from MCI to dementia. Alzheimer Dis Assoc Disord 2010; 24(1):-19-27.

41. Verfaillie SC, Adriaanse SM, Binnewijzend MA et al. Cerebral perfusion and glucose metabolism in Alzheimer's disease and frontotemporal dementia: two sides of the same coin? Eur Radiol 2015;
42. Taylor JP, Firbank MJ, He J et al. Visual cortex in dementia with Lewy bodies: magnetic resonance imaging study. Br J Psychiatry 2012; 200(6):-491-498.
43. Le Heron CJ, Wright SL, Melzer TR et al. Comparing cerebral perfusion in Alzheimer's disease and Parkinson's disease dementia: an ASL-MRI study. J Cereb Blood Flow Metab 2014; 34(6):-964-970.
44. Schuff N, Matsumoto S, Kmiecik J et al. Cerebral blood flow in ischemic vascular dementia and Alzheimer's disease, measured by arterial spin-labeling magnetic resonance imaging. Alzheimers Dement 2009; 5(6):-454-462.
45. Gao YZ, Zhang JJ, Liu H et al. Regional cerebral blood flow and cerebrovascular reactivity in Alzheimer's disease and vascular dementia assessed by arterial spinlabeling magnetic resonance imaging. Curr Neurovasc Res 2013; 10(1):-49-53.
46. Bastos-Leite AJ, Kuijer JP, Rombouts SA et al. Cerebral blood flow by using pulsed arterial spin-labeling in elderly subjects with white matter hyperintensities. AJNR Am J Neuroradiol 2008; 29(7):-1296-1301.
47. Firbank MJ, He J, Blamire AM et al. Cerebral blood flow by arterial spin labeling in poststroke dementia. Neurology 2011; 76(17):-1478-1484.
48. van Gelderen P, de Zwart JA, & Duyn JH. Pittfalls of MRI measurement

of white matter perfusion based on arterial spin labeling. Magn Reson Med 2008; 59(4):-788-795.

49. van Osch MJ, Teeuwisse WM, van Walderveen MA et al. Can arterial spin labeling detect white matter perfusion signal? Magn Reson Med 2009; 62(1):-165-173.
50. Wu WC, Lin SC, Wang DJ et al. Measurement of cerebral white matter perfusion using pseudocontinuous arterial spin labeling 3T magnetic resonance imaging--an experimental and theoretical investigation of feasibility. PLoS One 2013; 8(12):-e82679.
51. Tissue plasminogen activator for acute ischemic stroke. The National Institute of Neurological Disorders and Stroke rt-PA Stroke Study Group. N Engl J Med 1995; 333(24):-1581-1587.
52. Siewert B, Schlaug G, Edelman RR et al. Comparison of EPISTAR and T2*-weighted gadolinium-enhanced perfusion imaging in patients with acute cerebral ischemia. Neurology 1997; 48(3):-673-679.
53. Viallon M, Altrichter S, Pereira VM et al. Combined use of pulsed arterial spin-labeling and susceptibility-weighted imaging in stroke at 3T. Eur Neurol 2010; 64(5):-286-296.
54. Zaharchuk G, El Mogy IS, Fischbein NJ et al. Comparison of arterial spin labeling and bolus perfusion-weighted imaging for detecting mismatch in acute stroke. Stroke 2012; 43(7):-1843-1848.
55. Bokkers RP, Hernandez DA, Merino JG et al. Whole-brain arterial spin labeling perfusion MRI in patients with acute stroke. Stroke 2012; 43(5):-1290-1294.
56. Hernandez DA, Bokkers RP, Mirasol RV et al. Pseudocontinuous arterial

spin labeling quantifies relative cerebral blood flow in acute stroke. Stroke 2012; 43(3):-753-758.

57. Chng SM, Petersen ET, Zimine I et al. Territorial arterial spin labeling in the assessment of collateral circulation: comparison with digital subtraction angiography. Stroke 2008; 39(12):-3248-3254.
58. Zaharchuk G, Do HM, Marks MP et al. Arterial spin-labeling MRI can identify the presence and intensity of collateral perfusion in patients with moyamoya disease. Stroke 2011; 42(9):-2485-2491.
59. Altrichter S, Kulcsar Z, Jagersberg M et al. Arterial spin labeling shows cortical collateral flow in the endovascular treatment of vasospasm after post-traumatic subarachnoid hemorrhage. J Neuroradiol 2009; 36(3):-158-161.
60. Bivard A, Krishnamurthy V, Stanwell P et al. Arterial spin labeling versus bolus-tracking perfusion in hyperacute stroke. Stroke 2014; 45(1):-127-133.
61. Teeuwisse WM, Schmid S, Ghariq E et al. Time-encoded pseudocontinuous arterial spin labeling: basic properties and timing strategies for human applications. Magn Reson Med 2014; 72(6):-1712-1722.
62. Dai W, Shankaranarayanan A, & Alsop DC. Volumetric measurement of perfusion and arterial transit delay using hadamard encoded continuous arterial spin labeling. Magn Reson Med 2013; 69(4):-1014-1022.
63. Hendrikse J, van Osch MJ, Rutgers DR et al. Internal carotid artery occlusion assessed at pulsed arterial spin-labeling perfusion MR imaging at multiple delay times. Radiology 2004; 233(3):-899-904.

64. Bokkers RP, van der Worp HB, Mali WP et al. Noninvasive MR imaging of cerebral perfusion in patients with a carotid artery stenosis. Neurology 2009; 73(11):-869-875.
65. Noguchi T, Kawashima M, Irie H et al. Arterial spin-labeling MR imaging in moyamoya disease compared with SPECT imaging. Eur J Radiol 2011; 80(3):-e557-e562.
66. Saida T, Masumoto T, Nakai Y et al. Moyamoya disease: evaluation of postoperative revascularization using multiphase selective arterial spin labeling MRI. J Comput Assist Tomogr 2012; 36(1):-143-149.
67. Sugino T, Mikami T, Miyata K et al. Arterial spin-labeling magnetic resonance imaging after revascularization of moyamoya disease. J Stroke Cerebrovasc Dis 2013; 22(6):-811-816.
68. Goetti R, O'Gorman R, Khan N et al. Arterial spin labelling MRI for assessment of cerebral perfusion in children with moyamoya disease: comparison with dynamic susceptibility contrast MRI. Neuroradiology 2013; 55(5):-639-647.
69. Wolf RL, Wang J, Detre JA et al. Arteriovenous shunt visualization in arteriovenous malformations with arterial spin-labeling MR imaging. AJNR Am J Neuroradiol 2008; 29(4):-681-687.
70. Le TT, Fischbein NJ, Andre JB et al. Identification of venous signal on arterial spin labeling improves diagnosis of dural arteriovenous fistulas and small arteriovenous malformations. AJNR Am J Neuroradiol 2012; 33(1):-61-68.
71. Alexander M, McTaggart R, Santarelli J et al. Multimodality evaluation of dural arteriovenous fistula with CT angiography, MR with arterial spin

labeling, and digital subtraction angiography: case report. J Neuroimaging 2014; 24(5):-520-523.

72. Iv M, Fischbein NJ, & Zaharchuk G. Association of developmental venous anomalies with perfusion abnormalities on arterial spin labeling and bolus perfusion-weighted imaging. J Neuroimaging 2015; 25(2):-243-250.
73. Kopeinigg D, & Bammer R. Time-resolved angiography using inflow subtraction (TRAILS). Magn Reson Med 2014; 72(3):-669-678.
74. Nguyen D, Kapina V, Seeck M et al. Ictal hyperperfusion demonstrated by arterial spin-labeling MRI in status epilepticus. J Neuroradiol 2010; 37(4):-250-251.
75. Pendse N, Wissmeyer M, Altrichter S et al. Interictal arterial spin-labeling MRI perfusion in intractable epilepsy. J Neuroradiol 2010; 37(1):-60-63.
76. Lim YM, Cho YW, Shamim S et al. Usefulness of pulsed arterial spin labeling MR imaging in mesial temporal lobe epilepsy. Epilepsy Res 2008; 82(2-3):-183-189.
77. Storti SF, Boscolo Galazzo I, Del Felice A et al. Combining ESI, ASL and PET for quantitative assessment of drug-resistant focal epilepsy. Neuroimage 2014; 102 Pt 149-59.
78. Miyaji Y, Yokoyama M, Kawabata Y et al. Arterial spin-labeling magnetic resonance imaging for diagnosis of late seizure after stroke. J Neurol Sci 2014; 339(1-2):-87-90.
79. Toledo M, Munuera J, Salas-Puig X et al. Localisation value of ictal arterial spin-labelled sequences in partial seizures. Epileptic Disord 2011; 13(3):-336-339.

80. Blauwblomme T, Boddaert N, Chemaly N et al. Arterial Spin Labeling MRI: a step forward in non-invasive delineation of focal cortical dysplasia in children. Epilepsy Res 2014; 108(10):-1932-1939.
81. Aronen HJ, Gazit IE, Louis DN et al. Cerebral blood volume maps of gliomas: comparison with tumor grade and histologic findings. Radiology 1994; 191(1):-41-51.
82. Knopp EA, Cha S, Johnson G et al. Glial neoplasms: dynamic contrast-enhanced T2*-weighted MR imaging. Radiology 1999; 211(3):-791-798.
83. Cha S, Knopp EA, Johnson G et al. Dynamic contrast-enhanced T2-weighted MR imaging of recurrent malignant gliomas treated with thalidomide and carboplatin. AJNR Am J Neuroradiol 2000; 21(5):-881-890.
84. Sugahara T, Korogi Y, Kochi M et al. Correlation of MR imaging-determined cerebral blood volume maps with histologic and angiographic determination of vascularity of gliomas. AJR Am J Roentgenol 1998; 171(6):-1479-1486.
85. Cha S, Tihan T, Crawford F et al. Differentiation of low-grade oligodendrogliomas from low-grade astrocytomas by using quantitative blood-volume measurements derived from dynamic susceptibility contrast-enhanced MR imaging. AJNR Am J Neuroradiol 2005; 26(2):-266-273.
86. Roberts HC, Roberts TP, Bollen AW et al. Correlation of microvascular permeability derived from dynamic contrast-enhanced MR imaging with histologic grade and tumor labeling index: a study in human brain tumors. Acad Radiol 2001; 8(5):-384-391.

87. Patankar TF, Haroon HA, Mills SJ et al. Is volume transfer coefficient (K(trans)) related to histologic grade in human gliomas? AJNR Am J Neuroradiol 2005; 26(10):-2455-2465.
88. Grubb RLJ, Raichle ME, Eichling JO et al. The effects of changes in PaCO2 on cerebral blood volume, blood flow, and vascular mean transit time. Stroke 1974; 5(5):-630-639.
89. Warmuth C, Gunther M, & Zimmer C. Quantification of blood flow in brain tumors: comparison of arterial spin labeling and dynamic susceptibility-weighted contrast-enhanced MR imaging. Radiology 2003; 228(2):-523-532.
90. Wolf RL, Wang J, Wang S et al. Grading of CNS neoplasms using continuous arterial spin labeled perfusion MR imaging at 3 Tesla. J Magn Reson Imaging 2005; 22(4):-475-482.
91. Jarnum H, Steffensen EG, Knutsson L et al. Perfusion MRI of brain tumours: a comparative study of pseudo-continuous arterial spin labelling and dynamic susceptibility contrast imaging. Neuroradiology 2010; 52(4):-307-317.
92. Lehmann P, Monet P, de Marco G et al. A comparative study of perfusion measurement in brain tumours at 3 Tesla MR: Arterial spin labeling versus dynamic susceptibility contrast-enhanced MRI. Eur Neurol 2010; 64(1):-21-26.
93. Qiao XJ, Ellingson BM, Kim HJ et al. Arterial Spin-Labeling Perfusion MRI Stratifies Progression-Free Survival and Correlates with Epidermal Growth Factor Receptor Status in Glioblastoma. AJNR Am J Neuroradiol 2014;

94. Furtner J, Bender B, Braun C et al. Prognostic value of blood flow measurements using arterial spin labeling in gliomas. PLoS One 2014; 9(6):-e99616.
95. De Bazelaire C, Rofsky NM, Duhamel G et al. Arterial spin labeling blood flow magnetic resonance imaging for the characterization of metastatic renal cell carcinoma(1). Acad Radiol 2005; 12(3):-347-357.
96. Yamashita K, Yoshiura T, Hiwatashi A et al. Arterial spin labeling of hemangioblastoma: differentiation from metastatic brain tumors based on quantitative blood flow measurement. Neuroradiology 2012; 54(8):-809-813.
97. Sugahara T, Korogi Y, Tomiguchi S et al. Posttherapeutic intraaxial brain tumor: the value of perfusion-sensitive contrast-enhanced MR imaging for differentiating tumor recurrence from nonneoplastic contrast-enhancing tissue. AJNR Am J Neuroradiol 2000; 21(5):-901-909.
98. Henry RG, Vigneron DB, Fischbein NJ et al. Comparison of relative cerebral blood volume and proton spectroscopy in patients with treated gliomas. AJNR Am J Neuroradiol 2000; 21(2):-357-366.
99. Barajas RFJ, Chang JS, Segal MR et al. Differentiation of recurrent glioblastoma multiforme from radiation necrosis after external beam radiation therapy with dynamic susceptibility-weighted contrast-enhanced perfusion MR imaging. Radiology 2009; 253(2):-486-496.
100. Ozsunar Y, Mullins ME, Kwong K et al. Glioma recurrence versus radiation necrosis? A pilot comparison of arterial spin-labeled, dynamic susceptibility contrast enhanced MRI, and FDG-PET imaging. Acad Radiol 2010; 17(3):-282-290.

101. Choi YJ, Kim HS, Jahng GH et al. Pseudoprogression in patients with glioblastoma: added value of arterial spin labeling to dynamic susceptibility contrast perfusion MR imaging. Acta Radiol 2013; 54(4):-448-454.
102. Ho TC, Wu J, Shin DD et al. Altered cerebral perfusion in executive, affective, and motor networks during adolescent depression. J Am Acad Child Adolesc Psychiatry 2013; 52(10):-1076-1091.e2.
103. Orosz A, Jann K, Federspiel A et al. Reduced cerebral blood flow within the default-mode network and within total gray matter in major depression. Brain Connect 2012; 2(6):-303-310.
104. Raichle ME, MacLeod AM, Snyder AZ et al. A default mode of brain function. Proceedings of the National Academy of Sciences 2001; 98(2):-676.
105. Barkhof F, Haller S, & Rombouts SA. Resting-State Functional MR Imaging: A New Window to the Brain. Radiology 2014; 272(1):-29-49.
106. Duhameau B, Ferre JC, Jannin P et al. Chronic and treatment-resistant depression: a study using arterial spin labeling perfusion MRI at 3Tesla. Psychiatry Res 2010; 182(2):-111-116.
107. Lui S, Parkes LM, Huang X et al. Depressive disorders: focally altered cerebral perfusion measured with arterial spin-labeling MR imaging. Radiology 2009; 251(2):-476-484.
108. Colloby SJ, Firbank MJ, He J et al. Regional cerebral blood flow in late-life depression: arterial spin labelling magnetic resonance study. Br J Psychiatry 2012; 200(2):-150-155.
109. Pinkham A, Loughead J, Ruparel K et al. Resting quantitative cerebral

blood flow in schizophrenia measured by pulsed arterial spin labeling perfusion MRI. Psychiatry Res 2011; 194(1):-64-72.

110. Ota M, Ishikawa M, Sato N et al. Pseudo-continuous arterial spin labeling MRI study of schizophrenic patients. Schizophr Res 2014; 154(1-3):-113-118.
111. Schuff N, Zhang Y, Zhan W et al. Patterns of altered cortical perfusion and diminished subcortical integrity in posttraumatic stress disorder: an MRI study. Neuroimage 2011; 54 Suppl 1S62-S68.
112. Li X, Spence JS, Buhner DM et al. Hippocampal dysfunction in Gulf War veterans: investigation with ASL perfusion MR imaging and physostigmine challenge. Radiology 2011; 261(1):-218-225.
113. Grossman EJ, Jensen JH, Babb JS et al. Cognitive impairment in mild traumatic brain injury: a longitudinal diffusional kurtosis and perfusion imaging study. AJNR Am J Neuroradiol 2013; 34(5):-951-7, S1.
114. Ge Y, Patel MB, Chen Q et al. Assessment of thalamic perfusion in patients with mild traumatic brain injury by true FISP arterial spin labelling MR imaging at 3T. Brain Inj 2009; 23(7):-666-674.
115. Doshi H, Wiseman N, Liu J et al. Cerebral hemodynamic changes of mild traumatic brain injury at the acute stage. PLoS One 2015; 10(2):-e0118061.
116. Wang Y, West JD, Bailey JN et al. Decreased Cerebral Blood Flow in Chronic Pediatric Mild TBI: An MRI Perfusion Study. Dev Neuropsychol 2015; 40(1):-40-44.
117. Owen DG, Bureau Y, Thomas AW et al. Quantification of pain-induced changes in cerebral blood flow by perfusion MRI. Pain 2008; 136(1-2):-

85-96.

118. Liu J, Hao Y, Du M et al. Quantitative cerebral blood flow mapping and functional connectivity of postherpetic neuralgia pain: a perfusion fMRI study. Pain 2013; 154(1):-110-118.
119. Kato Y, Araki N, Matsuda H et al. Arterial spin-labeled MRI study of migraine attacks treated with rizatriptan. J Headache Pain 2010; 11(3):-255-258.
120. Pollock JM, Deibler AR, Burdette JH et al. Migraine associated cerebral hyperperfusion with arterial spin-labeled MR imaging. AJNR Am J Neuroradiol 2008; 29(8):-1494-1497.
121. Zaharchuk G, Ledden PJ, Kwong KK et al. Multislice perfusion and perfusion territory imaging in humans with separate label and image coils. Magn Reson Med 1999; 41(6):-1093-1098.
122. Hendrikse J, van der Grond J, Lu H et al. Flow territory mapping of the cerebral arteries with regional perfusion MRI. Stroke 2004; 35(4):-882-887.
123. Hendrikse J, Petersen ET, Chng SM et al. Distribution of cerebral blood flow in the nucleus caudatus, nucleus lentiformis, and thalamus: a study of territorial arterial spin-labeling MR imaging. Radiology 2010; 254(3):-867-875.
124. Gupta A, Chazen JL, Hartman M et al. Cerebrovascular reserve and stroke risk in patients with carotid stenosis or occlusion: a systematic review and meta-analysis. Stroke 2012; 43(11):-2884-2891.
125. Bokkers RP, van Osch MJ, van der Worp HB et al. Symptomatic carotid artery stenosis: impairment of cerebral autoregulation measured at the

brain tissue level with arterial spin-labeling MR imaging. Radiology 2010; 256(1):-201-208.

126. Ogawa S, Lee TM, Kay AR et al. Brain magnetic resonance imaging with contrast dependent on blood oxygenation. Proc Natl Acad Sci U S A 1990; 87(24):-9868-9872.
127. Villringer A, & Dirnagl U. Coupling of brain activity and cerebral blood flow: basis of functional neuroimaging. Cerebrovasc Brain Metab Rev 1995; 7(3):-240-276.
128. Gauthier CJ, Madjar C, Desjardins-Crepeau L et al. Age dependence of hemodynamic response characteristics in human functional magnetic resonance imaging. Neurobiol Aging 2013; 34(5):-1469-1485.
129. Tjandra T, Brooks JC, Figueiredo P et al. Quantitative assessment of the reproducibility of functional activation measured with BOLD and MR perfusion imaging: implications for clinical trial design. Neuroimage 2005; 27(2):-393-401.
130. Heijtel DF, Mutsaerts HJ, Bakker E et al. Accuracy and precision of pseudo-continuous arterial spin labeling perfusion during baseline and hypercapnia: a head-to-head comparison with (1)(5)O H(2)O positron emission tomography. Neuroimage 2014; 92182-192.
131. Kilroy E, Apostolova L, Liu C et al. Reliability of two-dimensional and three-dimensional pseudo-continuous arterial spin labeling perfusion MRI in elderly populations: comparison with 15O-water positron emission tomography. J Magn Reson Imaging 2014; 39(4):-931-939.
132. Zhang K, Herzog H, Mauler J et al. Comparison of cerebral blood flow acquired by simultaneous [15O]water positron emission tomography and

arterial spin labeling magnetic resonance imaging. J Cereb Blood Flow Metab 2014; 34(8):-1373-1380.

133. Stegger L, Martirosian P, Schwenzer N et al. Simultaneous PET/MR imaging of the brain: feasibility of cerebral blood flow measurements with FAIR-TrueFISP arterial spin labeling MRI. Acta Radiol 2012; 53(9):-1066-1072.
134. Qiu M, Paul Maguire R, Arora J et al. Arterial transit time effects in pulsed arterial spin labeling CBF mapping: insight from a PET and MR study in normal human subjects. Magn Reson Med 2010; 63(2):-374-384.
135. Lövblad KO, Montandon ML, Viallon M et al. Arterial Spin-Labeling Parameters Influence Signal Variability and Estimated Regional Relative Cerebral Blood Flow in Normal Aging and Mild Cognitive Impairment: FAIR versus PICORE Techniques. AJNR Am J Neuroradiol 2015;
136. Asllani I, Borogovac A, & Brown TR. Regression algorithm correcting for partial volume effects in arterial spin labeling MRI. Magn Reson Med 2008; 60(6):-1362-1371.
137. Petersen ET, Mouridsen K, & Golay X. The QUASAR reproducibility study, Part II: Results from a multi-center Arterial Spin Labeling test-retest study. Neuroimage 2010; 49(1):-104-113.
138. Gevers S, van Osch MJ, Bokkers RP et al. Intra- and multicenter reproducibility of pulsed, continuous and pseudo-continuous arterial spin labeling methods for measuring cerebral perfusion. J Cereb Blood Flow Metab 2011; 31(8):-1706-1715.
139. Mutsaerts HJ, van Osch MJ, Zelaya FO et al. Multi-vendor reliability of

arterial spin labeling perfusion MRI using a near-identical sequence: Implications for multi-center studies. Neuroimage 2015; 113143-152.

140. Fernandez-Seara MA, Wang Z, Wang J et al. Continuous arterial spin labeling perfusion measurements using single shot 3D GRASE at 3 T. Magn Reson Med 2005; 54(5):-1241-1247.
141. Gai ND, Talagala SL, & Butman JA. Whole-brain cerebral blood flow mapping using 3D echo planar imaging and pulsed arterial tagging. J Magn Reson Imaging 2011; 33(2):-287-295.
142. Vidyasagar R, Greyling A, Draijer R et al. The effect of black tea and caffeine on regional cerebral blood flow measured with arterial spin labeling. J Cereb Blood Flow Metab 2013; 33(6):-963-968.
143. Haller S, Rodriguez C, Moser D et al. Acute caffeine administration impact on working memory-related brain activation and functional connectivity in the elderly: a BOLD and perfusion MRI study. Neuroscience 2013; 250364-371.
144. Haller S, Montandon ML, Rodriguez C et al. Acute Caffeine Administration Effect on Brain Activation Patterns in Mild Cognitive Impairment. J Alzheimers Dis 2014; 41(1):-101-112.
145. Lu H, Clingman C, Golay X et al. Determining the longitudinal relaxation time (T1) of blood at 3.0 Tesla. Magn Reson Med 2004; 52(3):-679-682.
146. Varela M, Hajnal JV, Petersen ET et al. A method for rapid in vivo measurement of blood T1. NMR Biomed 2011; 24(1):-80-88.
147. Varela M, Petersen ET, Golay X et al. Cerebral blood flow measurements in infants using look-locker arterial spin labeling. J Magn Reson Imaging 2014;

148. Oguz KK, Golay X, Pizzini FB et al. Sickle cell disease: continuous arterial spin-labeling perfusion MR imaging in children. Radiology 2003; 227(2):-567-574.

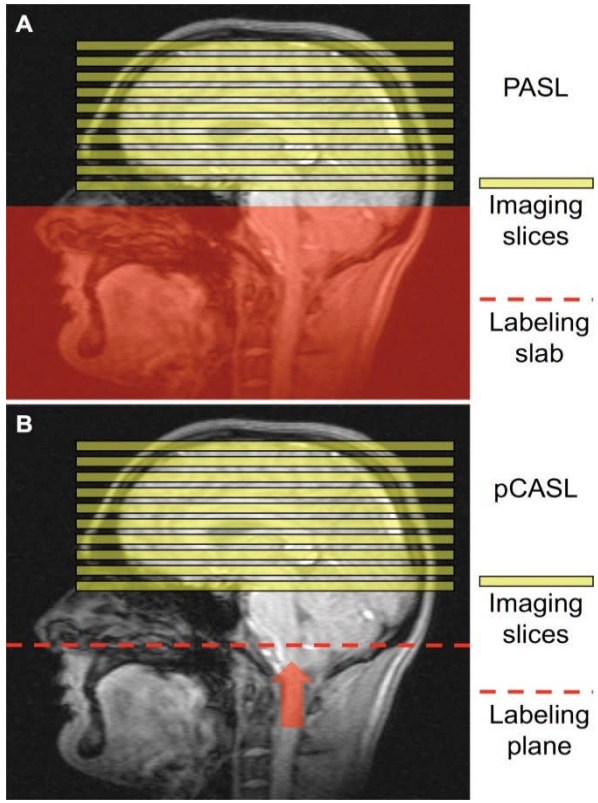

Figure 1 ASLarterial spin labeling labeling schemes. A, In PASLpulsed ASL, an inversion slab is placed proximal to the imaging volume to label blood in the arterial feeding vessels supplying the brain. The pulse is short (~10 msec) and all the blood is inverted simultaneously. B, In PCASLpseudocontinuous ASL, the inflowing arterial blood is continuously inverted as it flows through the labeling plane by means of a process known as flow-induced adiabatic inversion. The PCASLpseudocontinuous ASL labeling pulse train is typically applied for a period of approximately 1–2 seconds.

,

.

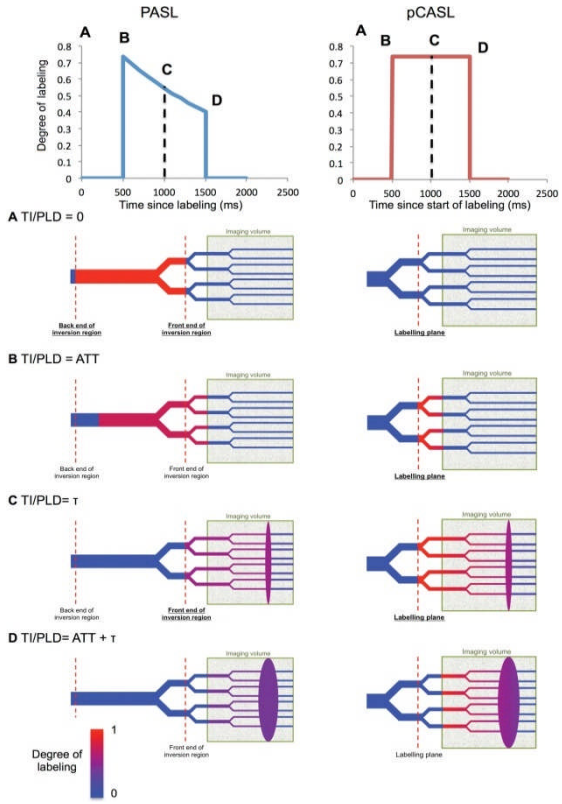

Figure 2 Differences in labeling degree of ASLarterial spin labeling bolus for PASLpulsed ASL (left column) and PCASLpseudocontinuous ASL (right column). The top row shows the temporal profile of the bolus (1 = fully inverted; 0 = fully relaxed). Since the PASLpulsed ASL inversion slab is inverted at a single point in time (t = 0 on this graph), all the inflowing arterial blood undergoes the same amount of T1 recovery at all time points after this. In PCASLpseudocontinuous ASL, blood is labeled as it flows through the inversion plane and recovers en route to the imaging volume. A–D show the degree of labeling remaining at several time points after the start of labeling (t = 0): A, t = 0; B, t = arterial arrival time (ATT); C, t = bolus duration (τ); D, t = ATT + τ. Color scale represents the range from fully inverted (red) to fully relaxed (blue). It can be seen that the PCASLpseudocontinuous ASL labeling process produces a bolus with a higher overall degree of inversion than does the PASLpulsed ASL, resulting in a higher intrinsic SNRsignal-to-noise ratio for PCASLpseudocontinuous ASL.

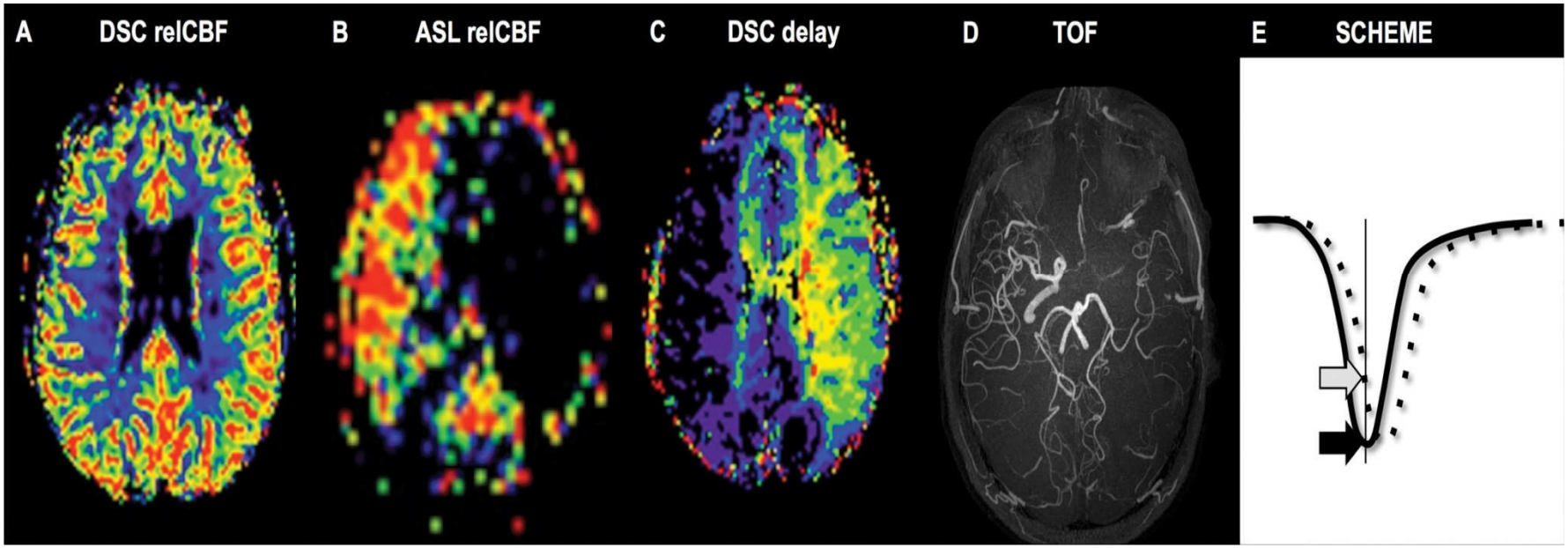

Figure 3 Example of an underestimation of relative CBFcerebral blood flow (relCBF) in ASLarterial spin labeling due to a proximal vessel stenosis. A, The estimated relative CBFcerebral blood flow based on DSCdynamic susceptibility contrast perfusion is within normal limits. B, In contrast, the relative CBFcerebral blood flow estimated by using a standard single–inflow-time ASLarterial spin labeling sequence demonstrates marked reduction in the left anterior and middle cerebral artery territories. The origin of this discrepancy is the increased perfusion delay, illustrated on, C, DSCdynamic susceptibility contrast-derived delay map, which exactly matches the altered perfusion in ASLarterial spin labeling due to the presence of a high-grade stenosis of the left internal carotid artery on, D, time-of-flight (TOF) image. The underlying principle is explained in E. The normal perfusion time series of DSCdynamic susceptibility contrast imaging (solid black line) is shifted to the right due to the presence of a proximal vessel stenosis and slower collateral flow (dotted line). DSCdynamic susceptibility contrast imaging acquires an entire time series, this shift in the bolus arrival simply causes a shift of the estimated curve, and the relative CBFcerebral blood flow can be accurately estimated in DSCdynamic susceptibility contrast. In contrast, a single–inflow-time ASLarterial spin labeling sequence with a standard inflow time (indicated by the vertical line) will underestimate the true perfusion simply because it is too early with respect to the peak of the perfusion curve.

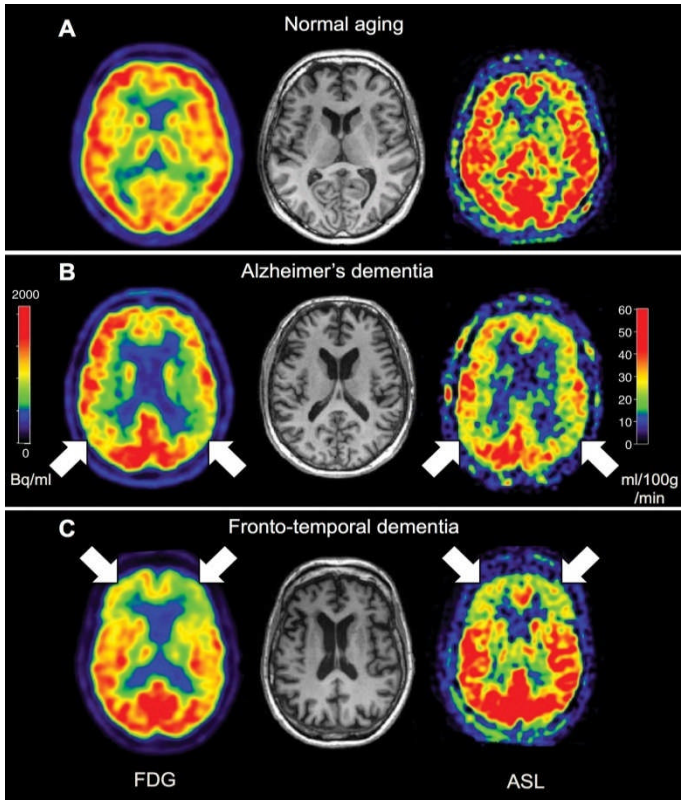

Figure 4 Examples of dementia. Transverse FDGfluorine 18 fluorodeoxyglucose and ASLarterial spin labeling images of, A, a healthy individual (male; age, 57 years; Mini-Mental State Examination [MMSE] score, 30), B, patient with ADAlzheimer disease (male; age, 52 years; MMSE score, 19), and, C, patient with frontotemporal lobar dementia (female; age, 53 years; MMSE score, 26). Functional images show predominant prefrontal abnormalities in FTD and parietal abnormalities in ADAlzheimer disease. Red color reflects normal metabolism and perfusion.

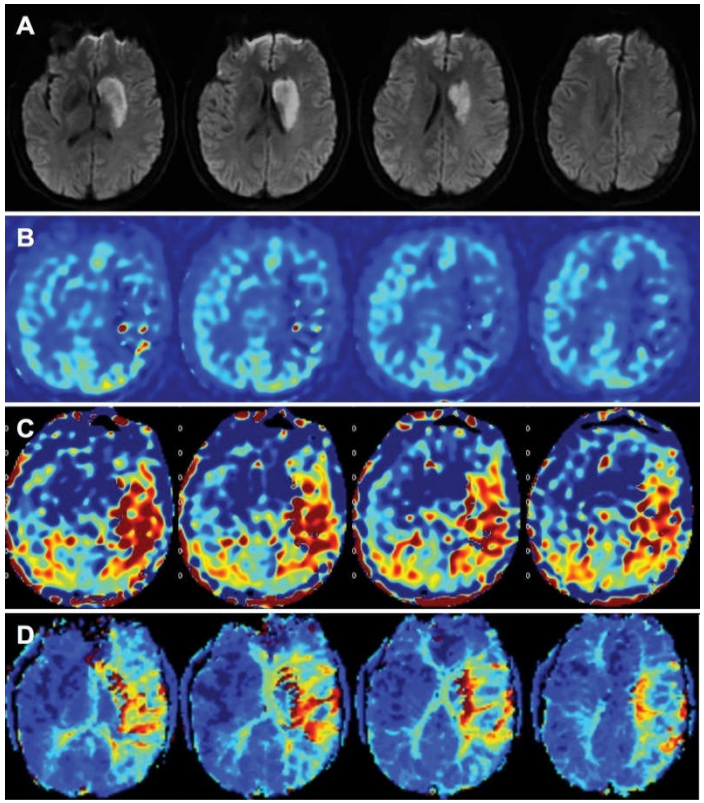

Figure 5 Images in 50-year-old woman presenting with stroke, with 14 hours of right hemiparesis and aphasia, National Institutes of Health Stroke Scale score of 9 at the time of imaging. Patient was later found to have extracranial left internal carotid artery dissection. A, Diffusion-weighted images demonstrate irreversibly damaged tissue within the left caudate and putamen. By using a multidelay ASLarterial spin labeling sequence capable of acquiring both, B, CBFcerebral blood flow and, C, arterial transit time images, a larger region of perfusion abnormality is identified. D, Conventional DSCdynamic susceptibility contrast images show the region of perfusion abnormality (time to the maximum of the residue function) is concordant with the findings on ASLarterial spin labeling images.

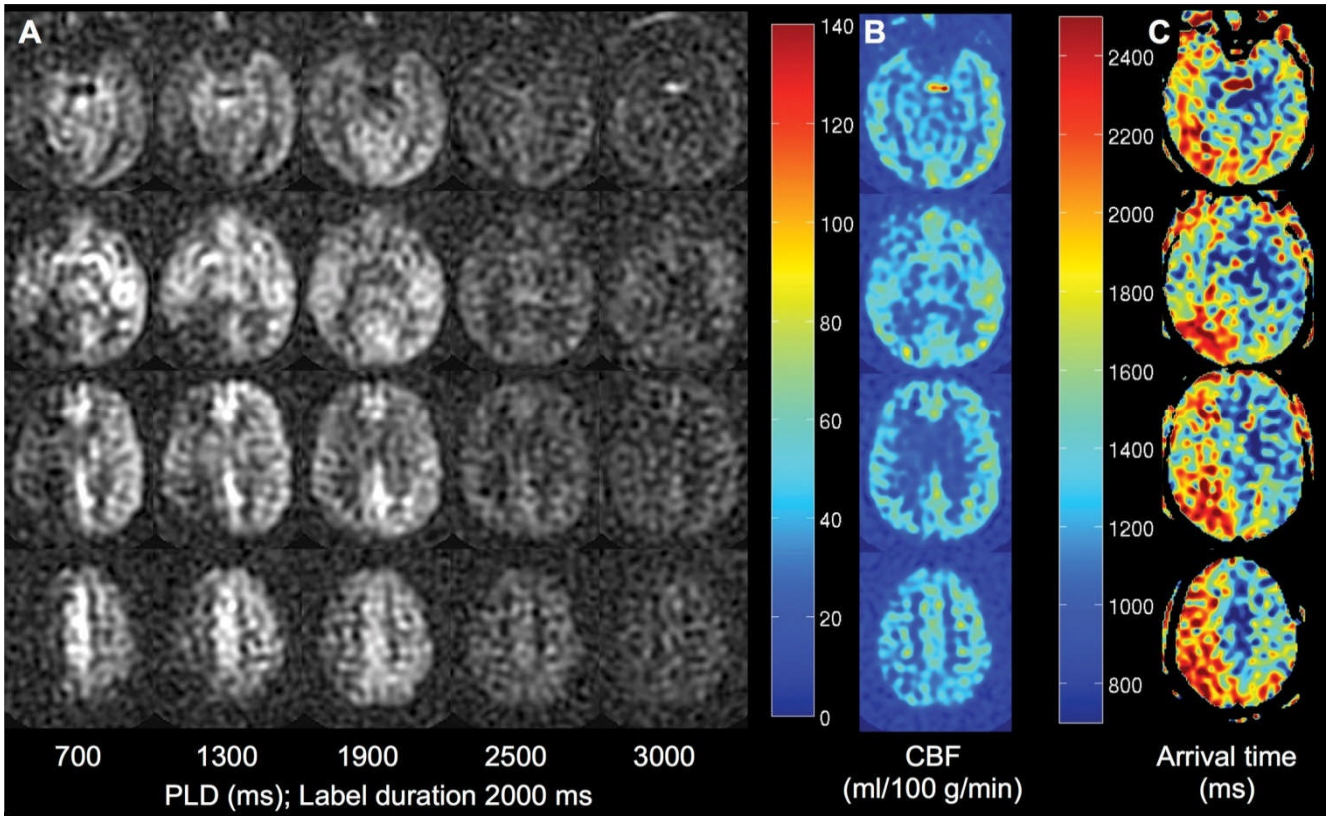

Figure 6 Example of multidelay ASLarterial spin labeling imaging. A fixed labeling duration of 2000 msec is used, but on subsequent images, different postlabel delays (PLD) ranging from 700 to 3000 msec are used, yielding ASLarterial spin labeling difference (control label) images as shown in A. From these data, and the use of general kinetic modeling, one can simultaneously measure, B, an arrival-time–corrected CBFcerebral blood flow and, C, the arterial arrival time itself. In this patient, there is near symmetric CBFcerebral blood flow but clear arterial arrival delay in the right hemisphere, as shown by the higher values on the arrival time map.

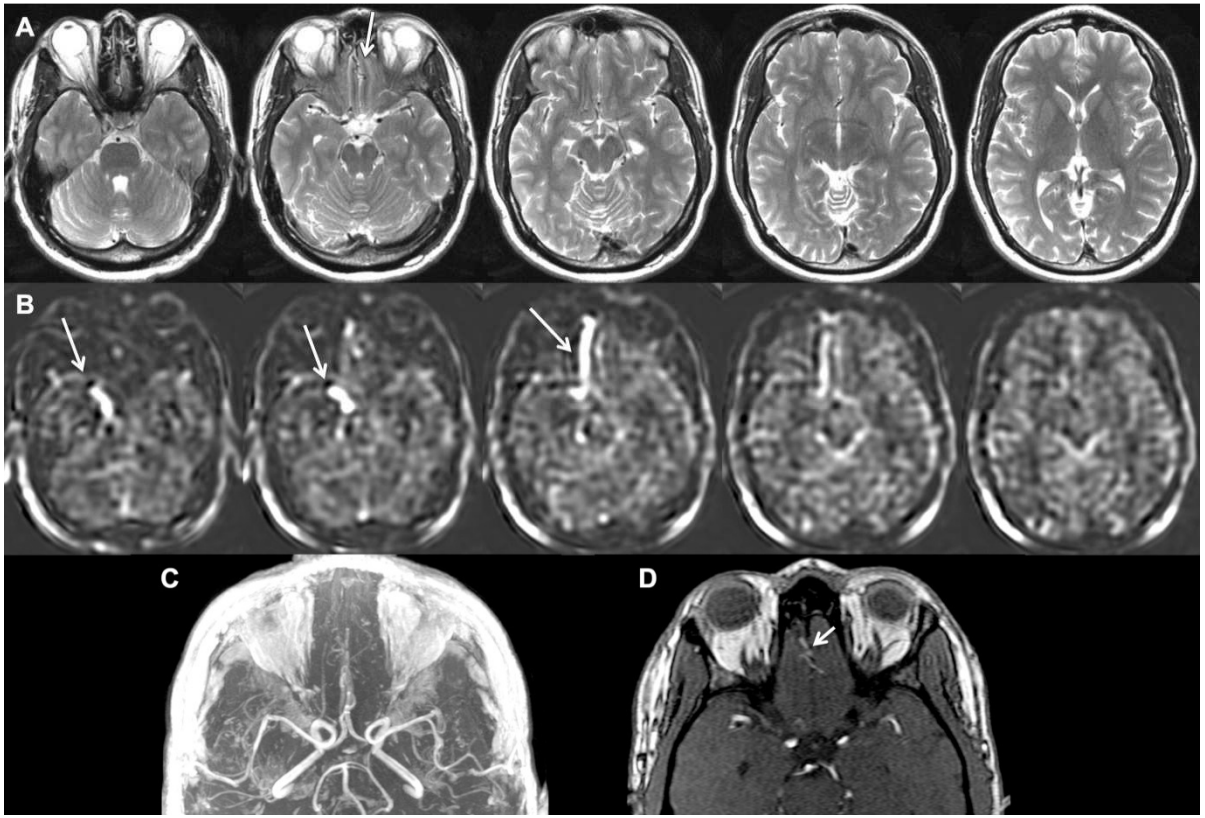

Figure 7 Images in 51-year-old man with exertional headaches and an arteriovenous fistula imaged at 1.5 T. A, T2-weighted images demonstrate very subtle flow voids in the inferior frontal lobe (arrow). B, ASLarterial spin labeling images demonstrate linear high signal intensity (arrows) in the region of the right inferior frontal lobe, which extends to the right cavernous sinus, indicative of an arteriovenous shunt lesion. C, Collapsed and, D, source MR angiographic images confirm the presence of an ethmoid dural fistula (arrow), which was recognized only after the observation of the abnormal ASLarterial spin labeling signal within the venous structures draining the fistula. This case also demonstrates that while 3 T is preferable to 1.5 T, relevant clinical information can be obtained with ASLarterial spin labeling at 1.5 T.

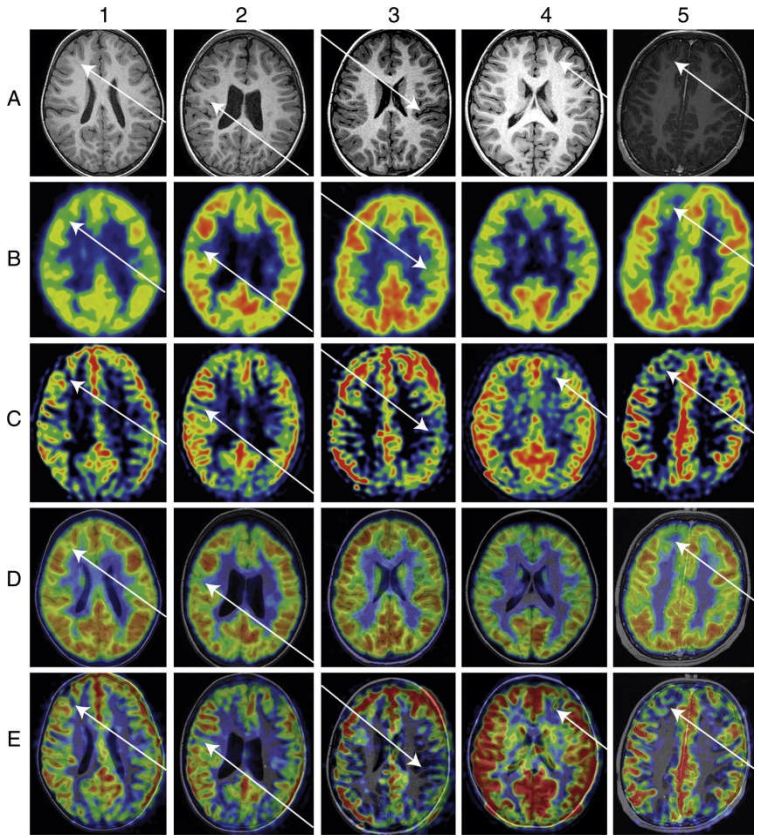

Figure 8 Comparison of ASLarterial spin labeling MR imaging and FDGfluorine 18 fluorodeoxyglucose PET in epilepsy. Each column represents imaging studies of a single patient. A, Preoperative axial T1-weighted MR images. B, Raw FDGfluorine 18 fluorodeoxyglucose PET images. C, Raw PASLpulsed ASL CBFcerebral blood flow maps. D, Image fusion of T1-weighted MR imaging and FDGfluorine 18 fluorodeoxyglucose PET. E, Image fusion of T1-weighted MR imaging and PASLpulsed ASL. Arrows indicate regions of focal cortical dysplasia that are epileptogenic. Numbers 1–5 refer to different patients. (Reprinted, with permission, from reference 80.)

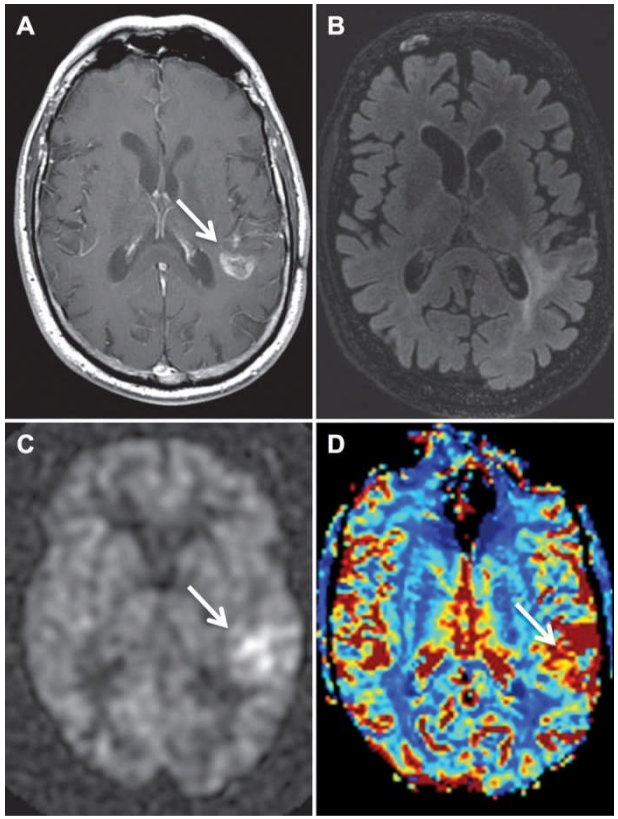

Figure 9 Images in 78-year-old man with unresectable anaplastic astrocytoma (arrow) (World Health Organization Grade 3), seen on, A, postcontrast T1-weighted and, B, FLAIR images. C, ASLarterial spin labeling image demonstrates increased CBFcerebral blood flow (arrow) in the region of the tumor. D, Increased cerebral blood volume (arrow) is also visible on bolus DSCdynamic susceptibility contrast image, though it is more difficult to appreciate due to the extensive number of arterial and venous vessels that surround the tumor. The findings of high CBFcerebral blood flow are characteristic of high-grade (grades III and IV) glial neoplasms.

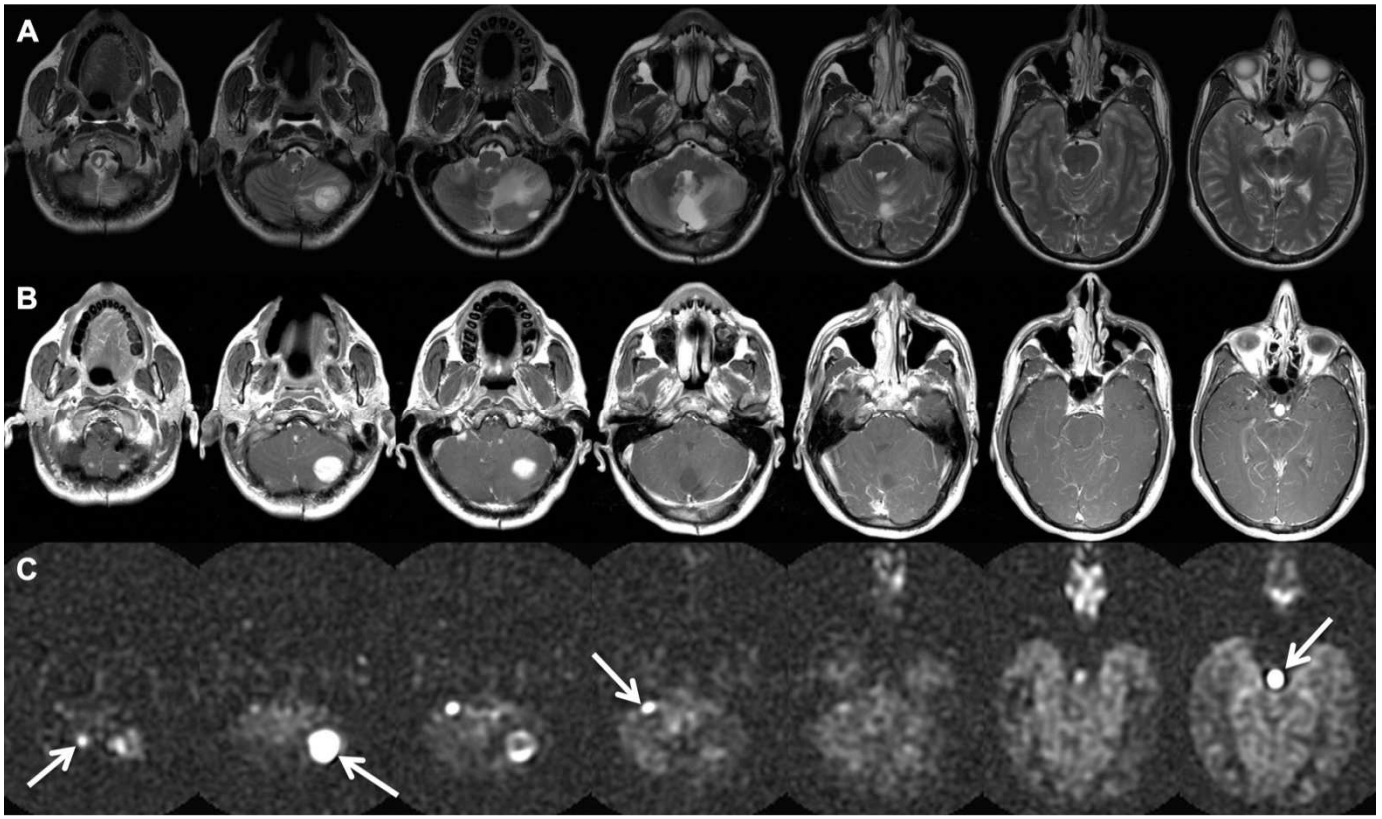

Figure 10 A, T2-weighted, B, postcontrast T1-weighted, and C, ASLarterial spin labeling images in a 40-year-old man with von Hippel Lindau disease and multiple hemangioblastomas after multiple prior surgeries. Arrows point to the extremely high CBFcerebral blood flow measured with ASLarterial spin labeling even in very small lesions.

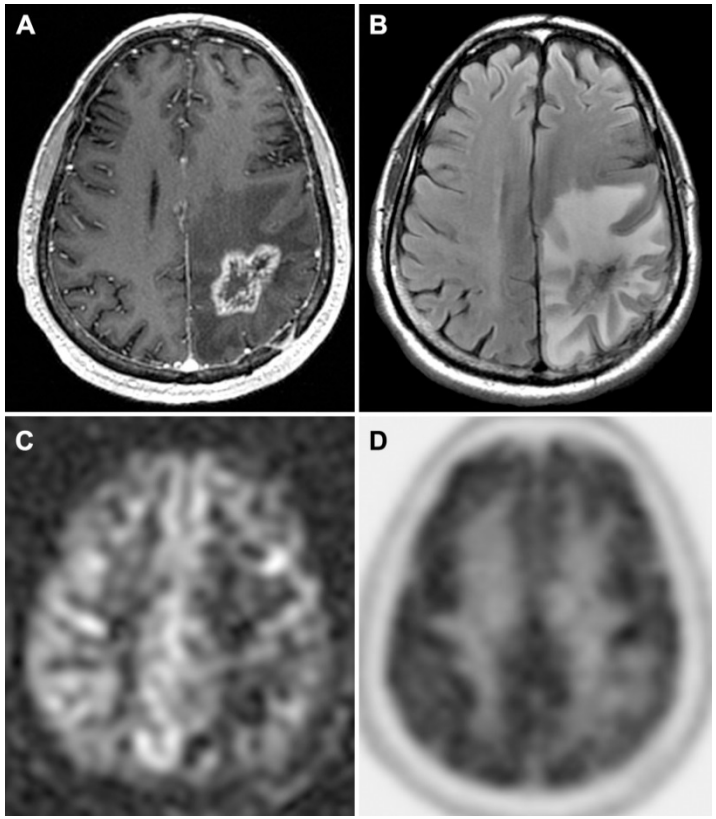

Figure 11 Images in 57-year-old man with lung cancer brain metastasis 15 months after resection, radiation, and chemotherapy. A, Axial T1-weighted gadolinium-enhanced image shows a new enhancing lesion, with, B, axial fluid-attenuated inversion recovery image demonstrating extensive vasogenic edema in the region of the resection cavity. C, ASLarterial spin labeling image demonstrates no increase in CBFcerebral blood flow in this region, similar to findings on, D, FDGfluorine 18 fluorodeoxyglucose PET image. These findings were considered to represent radiation necrosis and the patient is being followed serially rather than with re-resection.

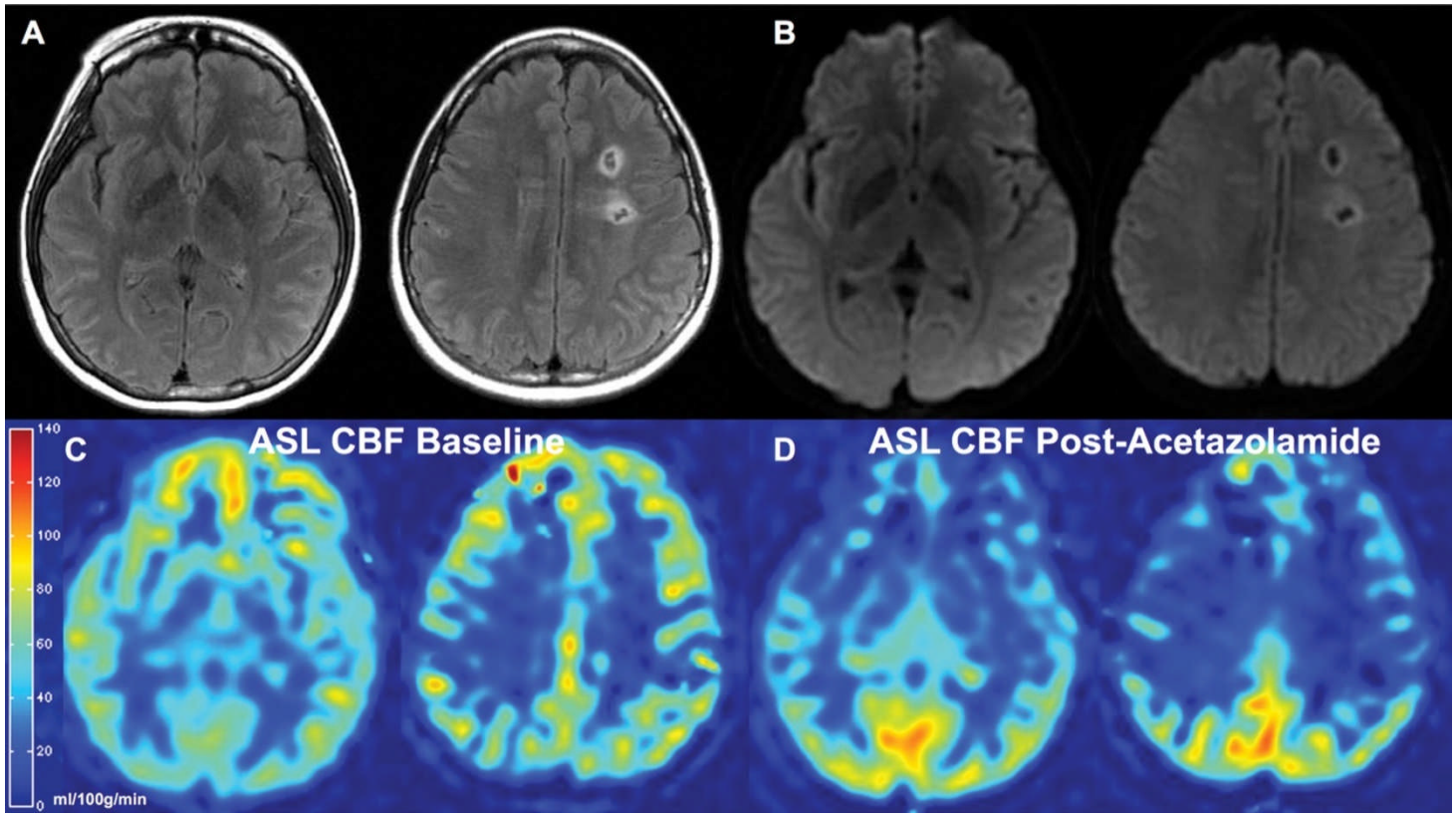

Figure 12 Images in 29-year-old woman with bilateral Moyamoya disease. Both, A, fluid-attenuated inversion recovery and, B, diffusion-weighted images show evidence of prior infarcts in the deep white matter on the left side. C, Multidelay ASLarterial spin labeling image acquired at baseline shows normal CBFcerebral blood flow in the bilateral anterior circulation. D, However, image obtained 10 minutes after intravenous administration of 1 g of acetazolamide demonstrates the expected CBFcerebral blood flow increase in the posterior circulation but marked reduction in CBFcerebral blood flow in both anterior circulations, compatible with cerebrovascular steal. This finding has been associated with a high risk of subsequent cerebrovascular events and prompted bilateral direct superficial temporal artery-middle cerebral artery bypass.

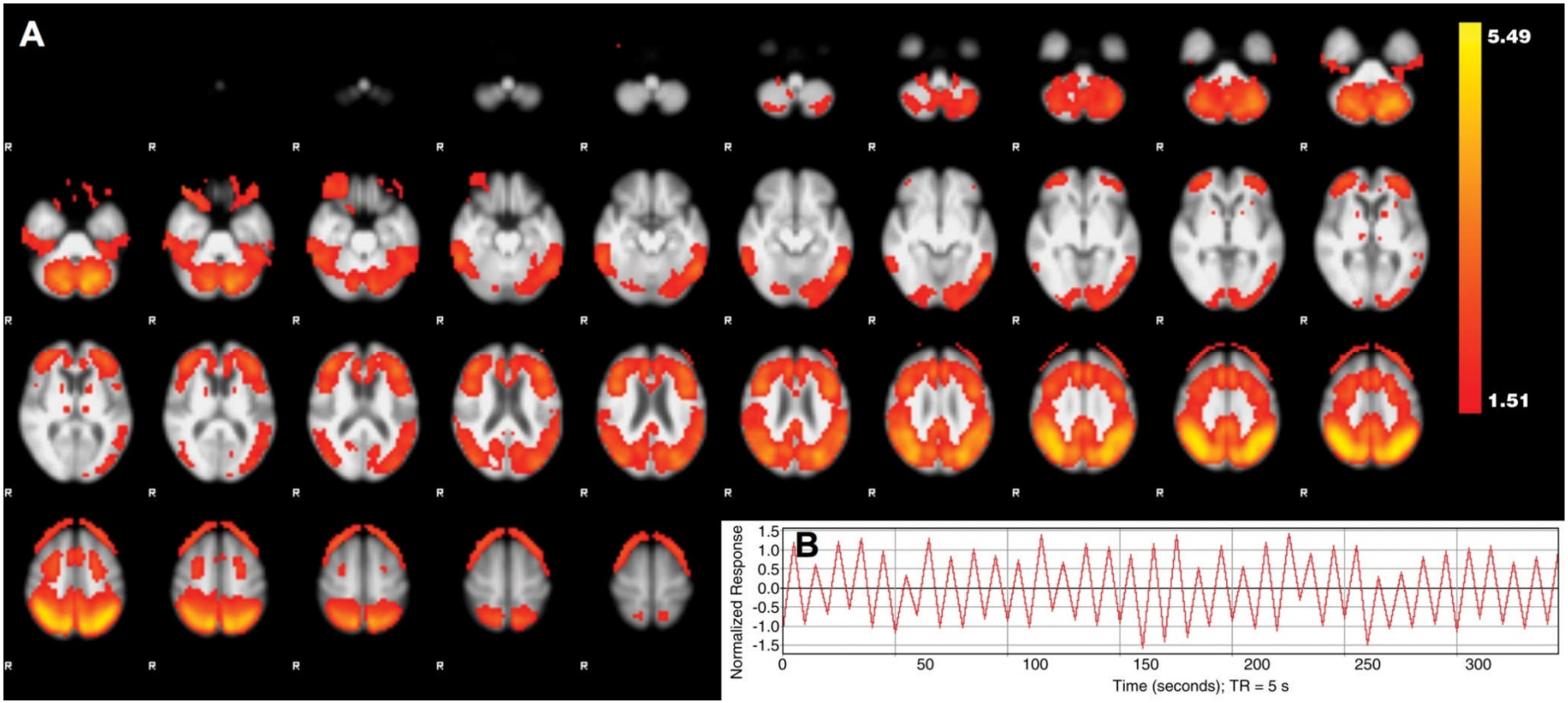

Figure 13 Functional connectivity analysis of ASLarterial spin labeling raw data in 154 healthy elderly control subjects and 66 cases with mild cognitive impairment. Note that for illustrative purposes, the raw ASLarterial spin labeling data were directly analyzed by using tensorial independent component in FSL (www.fmrib.ox.ac.uk/fsl/), an established technique optimized for functional MR imaging analysis. A, Spatial representation of one of the independent components. B, The on-off labeling pattern of the raw ASLarterial spin labeling data is clearly visible on the corresponding temporal representation. Currently ongoing methodological adaptation and optimization to the specific properties of ASL data, such as implementing the known prior knowledge of the on-off time course, will improve the quality of ASL-derived functional connectivity networks.